SEDIMENTOLOGY the journal of the International Association of Sedimentologists

Sedimentology (2021) doi: 10.1111/sed.12936

Inferring time averaging and hiatus durations in the stratigraphic record of high-frequency depositional sequences

ADAM TOMAŠOVÝCH*, IVO GALLMETZER†, ALEXANDRA HASELMAIR† and MARTIN ZUSCHIN†

**Earth Science Institute, Slovak Academy of Sciences, Dúbravska cesta 9, 84005 Bratislava, Slovakia (E-mail: geoltoma@savba.sk)*

†Department of Palaeontology, University of Vienna, Althanstrasse 14, 1090 Vienna, Austria

Associate Editor – Christian Betzler

ABSTRACT

A sequence stratigraphic framework predicts that time averaging and hiatus durations will be long at times of fastest sea-level rise. This prediction does not necessarily apply to environments where carbonate production keeps up with sea-level rise and where undetected hiatuses decouple short-term from long-term sedimentation rates. The taphonomic clock, however, which measures the residence time of skeletal particles in the mixed layer, can estimate the duration of hiatuses if the rate of skeletal alteration is slow and if skeletal particles endure long-term exposure in the mixed layer. Here, time averaging is calibrated by using evidence from alteration of bivalves in a metre-scale Holocene sequence in the Adriatic Sea. In this sequence, transgressive molluscan lags, a maximum-flooding zone shell bed with bivalves, and highstand bryomol assemblages were all deposited under similar long-term sedimentation rates (*ca* 0.01 to 0.03 cm year^{-1}) and exhibit millennial time averaging. Median ages of valves stained by pyrite and cemented by high-magnesium calcitic micritic envelopes exceeding *ca* 1000 years indicate that: (i) these authigenic processes are slow in subsurface zones with reducing conditions (with prolonged sulphate reduction and carbonate ions sourced from dissolved shells in the surface zones); and (ii) subsurface micrite precipitation prolongs the disintegration half-lives of valves exhumed to surface zones from decades to millennia. The high abundance of stained valves, valves with micrite envelopes, and valves with composite alteration (encrusters and borers colonizing stained and cemented grains) thus identifies hiatuses and skeletal concentrations time-averaged to >1000 years. The upcore decrease in abundance of valves with composite alteration, coupled with temporally-constant long-term sedimentation rates and time averaging, indicates that a temporal decline in sediment exhumation was compensated by a decline in burial of skeletal carbonate produced by molluscs.

Keywords Adriatic Sea, condensation, hiatus duration, sequence stratigraphy, stratigraphic resolution, taphofacies, taphonomic clock, time averaging.

INTRODUCTION

Hiatuses and condensed intervals can be qualitatively detected in the stratigraphic record based on ichnological, cyclostratigraphic and geochemical signals (Moore *et al.*, 1978; Amorosi, 1995; Pemberton *et al.*, 2004; Caron *et al.*, 2005; Andrieu *et al.*, 2018; Kemp *et al.*, 2018; Amorosi & Sammartino, 2018; Weedon *et al.*, 2018; Jarochowska *et al.*, 2020). Nonetheless, hiatus durations are difficult to

determine in pre-Holocene successions (Hillgärtner, 1998; Meyers & Sageman, 2004; Catuneanu, 2019a,b; Davies *et al.*, 2019; Holbrook & Miall, 2020; Brigaud *et al.*, 2021). Moreover, theory-based predictions about the differences in hiatus durations between the subsets of systems tracts are not straightforward. Sequence-stratigraphic predictions that sediment supply (and thus net sedimentation rate) and time averaging of skeletal grains covary with changes in accommodation space, typically leading to high time averaging during times of fast sea-level rise, were confirmed in siliciclastic systems (Kidwell, 1986, 1989, 1991a; Naish & Kamp, 1997; Kondo *et al.*, 1998; Holland, 2000; Hendy *et al.*, 2006; Scarponi *et al.*, 2013). However, the effect of rapid sea-level rise on the formation of hiatuses and on time averaging of sedimentary particles at hiatal surfaces is not simple in mixed or in carbonate systems (Zecchin & Catuneanu, 2013, 2017; Paul & Lokier, 2017). First, the reduction in clastic input leading to sediment retrogradation during maximum flooding phases on shelves can be compensated by *in situ* carbonate aggradation or by shedding of carbonates (Schlager, 1991; Schlager *et al.*, 1994; Massari & D'Alessandro, 2012; Pomar & Haq, 2016). Second, sediment accumulation can be independent of relative sea-level change in settings detached from the clastic input. Identifying condensed levels is also difficult because: (i) empirical estimates of long-term sedimentation rates do not linearly scale down to short-term sedimentation rates due to hidden (undetected) hiatuses (Sadler, 1981; Clari *et al.*, 1995; Tipper, 2016; Trampush & Hajek, 2017); and (ii) bioturbation obliterates sedimentological or cyclostratigraphic evidence of condensation (O'Leary *et al.*, 2009; Tomašových *et al.*, 2019a). Stratigraphic variability in time averaging and hiatus durations within depositional sequences thus need to be independently constrained in mixed and in carbonate systems (Gómez Fernández & Fernández López, 1994; Hillgärtner *et al.*, 1998; Caron *et al.*, 2012; Strasser, 2015; Brady & Bowie, 2017; Nohl & Munnecke, 2019). One such constraint is represented by the type and magnitude of alteration that affects skeletal particles that are resistant to winnowing and dissolution.

Alteration of skeletal particles can be either destructive (reducing their durability, i.e. the ability to withstand damage and wear by bioerosion, dissolution, maceration or by other mechanisms) or constructive (increasing their durability by recrystallization, mineralogical transformation or by precipitation of authigenic cements). Skeletal particles are exposed to fast disintegration by bioerosion, maceration and dissolution in the surface levels of the mixed layer affected by aerobic degradation of organic matter and sulphide oxidation [taphonomic active zone (TAZ); Davies *et al.*, 1989; Green *et al.*, 1993; Kidwell, 1993; Best *et al.*, 2007; Powell *et al.*, 2011; Petro *et al.*, 2018]. Disintegration of skeletal particles tends to be slow or negligible in the subsurface, incompletely-mixed or transitional layer that is rarely irrigated by burrowers [sequestration zone (SZ); Olszewski, 2004; Tomašových *et al.*, 2019a). Long residence times of skeletal particles in these subsurface zones expose them to the accumulated reaction products generated by anaerobic degradation of organic matter (Hendry *et al.*, 2000; Macintyre & Aronson, 2006; Schiffbauer *et al.*, 2014) and to downward-diffusing carbonate ions liberated by shell dissolution in the surface TAZ (Wheeley *et al.*, 2008). Consequently, long-lasting iron reduction, sulphate reduction associated with pyrite precipitation, or anaerobic methane oxidation can affect skeletal alteration by inducing the precipitation of authigenic carbonate cements (Pufahl & Grimm, 2003; Cherns *et al.*, 2008; Dickson *et al.*, 2008; Godet, 2013; Plet *et al.*, 2016; Braga *et al.*, 2019). If skeletal particles transit rapidly through the TAZ and the SZ into the zone of final burial (historical layer) beyond the reach of burrowers or physical erosion, they can enter the stratigraphic record without any alteration. Accordingly, alteration of skeletal particles in the surface and subsurface zones of the mixed layer is predicted to be high in strongly time-averaged lags or hiatal concentrations (Fürsich, 1979; Fürsich *et al.*, 1992; Burns *et al.*, 2005; McLaughlin *et al.*, 2008; Taylor & Machent, 2010; Morad *et al.*, 2012; Caratelli *et al.*, 2021). Excluding alteration that is generated during deeper burial and compaction, the frequency of alteration in stratigraphic increments can thus represent a taphonomic clock (Flessa *et al.*, 1993; Kidwell, 1997; Scarponi *et al.*, 2017). This clock can be used to estimate the time averaging of sediments in depositional sequences. It can track the duration of hiatuses associated with lags in the stratigraphic record especially if: (i) alteration signatures develop slowly over long timescales; and (ii) skeletal particles do not disintegrate rapidly in the mixed layer (Tomašových *et al.*, 2014, 2016).

This study evaluates whether the taphonomic clock can detect the amount of time condensed in stratigraphic increments in a high-frequency carbonate–siliciclastic sequence in the northern Adriatic Sea (Brijuni). Specific goals are: (i) to estimate the rate of distinct alteration processes and to distinguish between surface and

subsurface alteration pathways; (ii) to identify signatures that can track time averaging of skeletal particles in the ancient stratigraphic record; and (iii) to assess whether carbonate sediment produced by heterozoan groups can compensate for sediment erosion within a sequence that was deposited under a fast, eustatically-driven sea-level rise during the Early–Middle Holocene and under a slow increase during the Late Holocene sea-level stabilization.

Relationship between hiatus duration, time averaging and sedimentation rate

Here, hiatuses refer to any breaks in sedimentation that lead to the formation of hiatal surfaces (including diastems) or thin condensed increments that contain durable skeletal particles (Dominici, 2001; Kowalewski & Bambach, 2003; Peters, 2006; Brady, 2018; García-Ramos & Zuschin, 2019). Geochronological dating of two superposed levels in a Holocene section differing in age, for example by *ca* 1000 years or by *ca* 10 000 years, can demonstrate that they are separated by a thin lag encompassing these durations. Importantly, this accuracy is not available in the pre-Holocene stratigraphic record (e.g. Kemp, 2012). Durable skeletal particles in the lag may represent the whole hiatus duration (for example, 1000 or 10 000 years), whereas fragile remains may merely represent the last subset of that duration (for example, 100 or 1000 years, respectively). The taphonomic clock based on assemblage-level alteration can thus measure the total hiatus duration in circumstances when skeletal particles are durable and persist in the lag or in the mixed layer during the entire omission phase.

To assess the conditions in which time averaging of skeletal particles can track the entire hiatus duration, conceptual relations between long-term sedimentation rate, time averaging and hiatus duration in three scenarios shown in Fig. 1 were explored. Long-term sedimentation rates (based on four dated levels) and time averaging are closely related when the sedimentation rate and the thickness of the mixed layer remain constant through time (Fig. 1A). In scenario A, time averaging can be estimated from the long-term sedimentation rate because it should be equal to an inverse of that rate divided by the thickness of the mixed layer. The assemblage-level alteration is expected to scale positively with the residence time of skeletal particles in the mixed layer. However, if the sedimentation rate varies through time, long-term sedimentation rates are not informative about variability in short-term sedimentation rates. This difference between long-term and short-term sedimentation rates occurs because: (i) erosional events remove the signal of former deposition; and (ii) bioturbation smears out the remaining variability (Fig. 1B and C; Jerolmack & Sadler, 2007; Straub *et al.*, 2020).

In scenarios B and C, phases with omission lead to the deposition of thin, condensed lags formed by durable particles, followed by rapid sedimentation. The rapidly deposited increments deposited after omission phases are thus shell-poor. Fragile sedimentary particles are not preserved, leading to a hiatus in their deposition. In scenario B, time averaging of skeletal particles in the condensed, shell-poor lag underestimates the total hiatus duration because skeletal particles that enter the mixed layer during the omission phase do not survive up to the onset of deposition. In scenario C, time averaging in the condensed, shell-rich lag accurately detects the total hiatus duration because coarse and durable skeletal particles are resistant to dissolution or erosion. This condition ensures that skeletal particles can accumulate in the mixed layer and that their time averaging can capture the total hiatus duration. This scenario also leads to higher assemblage-level alteration when compared to other scenarios because the omission followed by rapid burial prolongs the residence time of skeletal particles in the mixed layer relative to that expected under the same long-term sedimentation rate in A. The scenarios B and C can be discriminated from one another based on the geochronological estimates of sedimentation rate and time averaging at Brijuni. Time averaging of skeletal particles in the shell-rich lags will be equal to or even higher than time averaging computed from long-term sedimentation rate in C, whereas time averaging of particles in the shell-poor lags will be shorter than time averaging computed from long-term sedimentation rate in B.

METHODS

Setting and sediment cores

The analyzed sediment cores were collected on the south-west margin of the Brijuni Islands archipelago in the northern Adriatic Sea (Fig. 2A). This sea represents a microtidal, storm-dominated carbonate epicontinental sea with low clastic input (Fütterer, 1969; Juračić *et al.*, 1999; Zuschin & Stachowitsch, 2009;

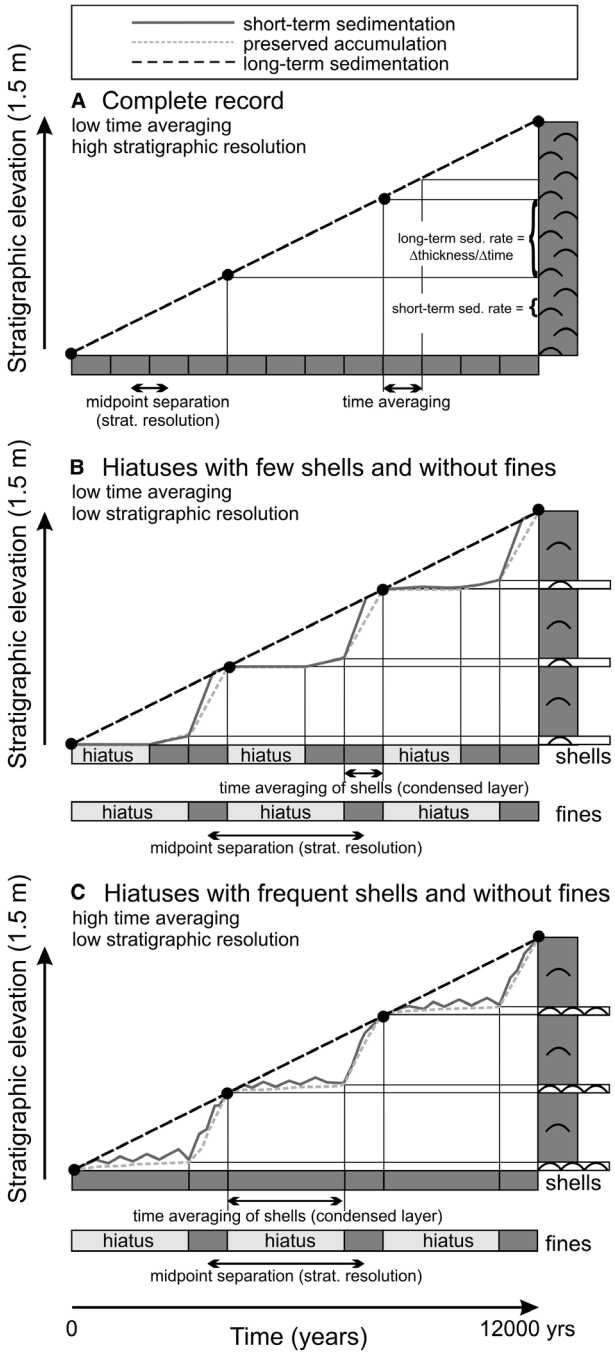

Fig. 1. Three scenarios with the same long-term sedimentation rate (dashed black lines, for example, 0.0125 cm year^{-1} if sedimentation takes places over 12 000 years) generating 1.5 m thick sections (vertical columns) differing in time averaging (horizontal arrows) and hiatus duration. Long-term sedimentation is based on four dated levels (black circles). (A) Sedimentation rate is constant through time. (B) and (C) Sedimentation rate varies through time. Long-term (black dashed lines) and short-term (grey shaded lines) sedimentation rates are decoupled in (B) and (C), and sediment fines (or fragile shells) are not preserved during the deposition of condensed lags. In (B) only a subset of shells is preserved in shell-poor lags at hiatal surfaces between rapidly-deposited units, and their time averaging thus does not track the entire hiatus duration. In (C) durable and highly altered shells form condensed shell-rich lags at hiatal surfaces and their time averaging tracks the entire hiatus duration. The residence time of shells in the shell-rich lags in (C) exceeds mean residence time predicted by the long-term sedimentation rate. Shell abundance in the sediment column on the right is based on a scenario where one shell enters the sediment–water interface per 1000 years.

Tomašových *et al.*, 2019b). Infralittoral habitats off the Istrian coast pass into low-angle, ramp-like circalittoral environments at *ca* 20 to 30 m (Jakl, 2012). Both infralittoral and circalittoral habitats along the Istrian coast are characterized by very low sedimentation rates, with a deposition of bryozoans, molluscs, coralline algae and echinoderms (with $CaCO_3$ exceeding 50%; Fütterer, 1969; Seneš, 1989). Four cores with 9 cm diameter were collected at water depths between 40 m and 44 m along a *ca* 80 m long transect with a piston corer in 2013 (Gallmetzer *et al.*, 2016). Sites located at these water depths were flooded about 11 000 years ago, with subsidence of *ca* 0.042 to 0.076 cm year^{-1} (Fig. 2B; Antonioli *et al.*, 2007). Two cores collected at 44 m depth are 155 to 160 cm long (cores M44 and M46) and two cores collected at 40 to 41 m depth are 95 to 120 cm long (cores M40 and M43; Fig. 2C). The core bottoms correspond to the wave-ravinement surface overlying muddy, organic-rich paralic deposits (Schnedl *et al.*, 2018). The cores were split into 2 cm increments in the upper 20 cm (analytically pooled into 4 cm) and into 5 cm increments below (Gallmetzer *et al.*, 2019).

Age data

Bivalve counts from 4 to 5 cm thick increments (sieved with 1 mm mesh size), grain-size data and geochronological data from M44 were presented by Schnedl *et al.* (2018) and Gallmetzer *et al.* (2019), including abundances of molluscan species, X-ray photographs and grain-size data (Figs 3 and 4). The determination of $CaCO_3$ content in the fine fraction (<63 μm) was based on the total inorganic carbon as measured by an elemental analyzer (CHN 2400, Perkin Elmer,

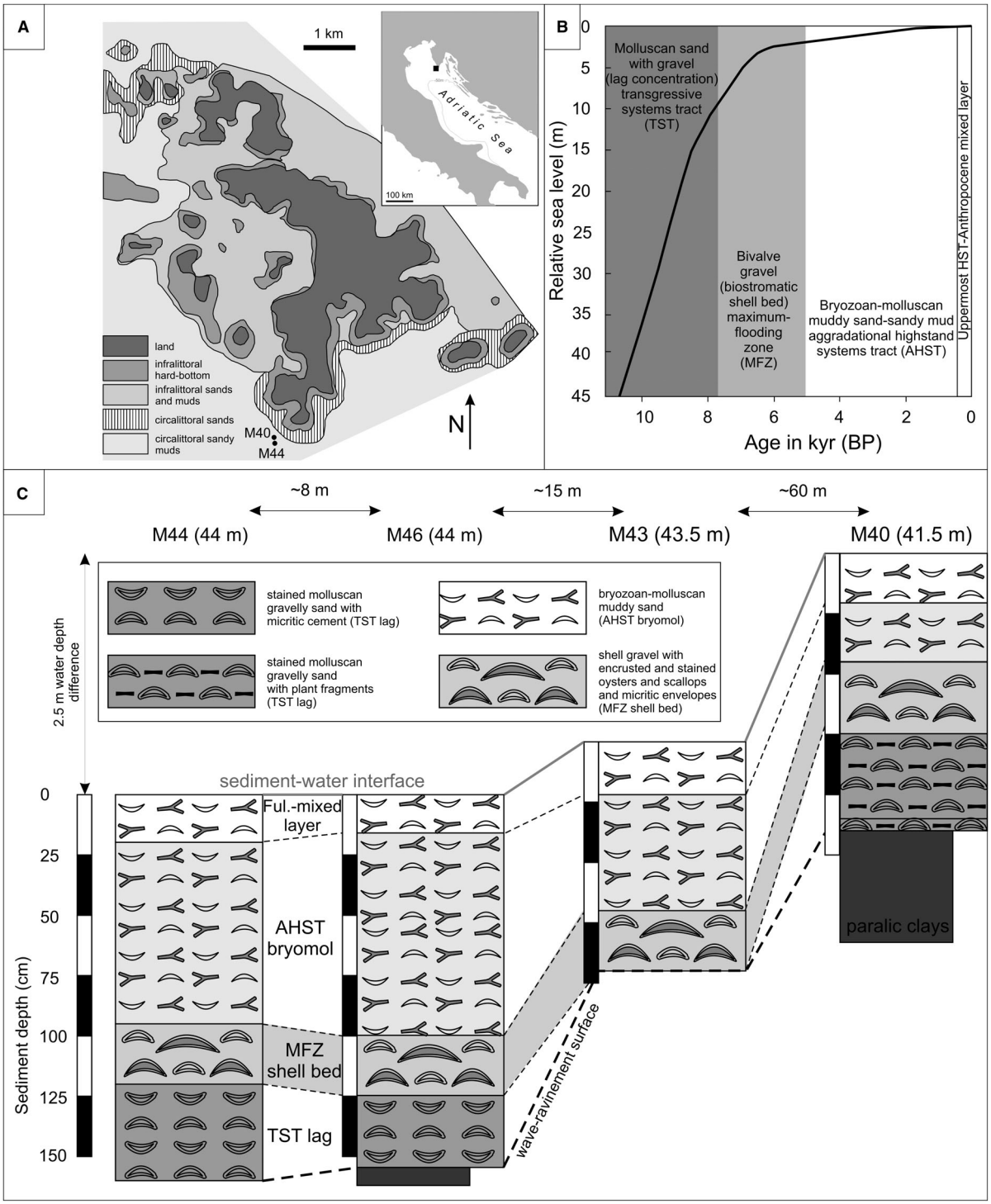

Fig. 2. (A) Geographic map of the Brijuni archipelago with infralittoral and circalittoral habitats (modified after Jakl, 2012) and the location of cores. The water depth steeply increases from island shorelines to rocky infralittoral habitats that terminate at *ca* 20 m. The seafloor at the coring stations is at 40 to 44 m depth. (B) The relative sea-level over the past 11 000 years for the Brijuni islands (Antonioli *et al.*, 2007), with approximate age ranges of the four stratigraphic units. (C) 95 to 160 cm long cores arranged along a *ca* 80 m long transect show variability in the thickness of transgressive (TST), maximum-flooding zone (MFZ) and aggradational–highstand units (AHST). The fully-mixed, age-homogenized layer corresponds to the upper 16 to 20 cm of the AHST. Cores M44 and M46 were collected at 44 m depth, core M40 at 41.5 m. The stratigraphic changes in grain size at M44 are shown in Fig. 4.

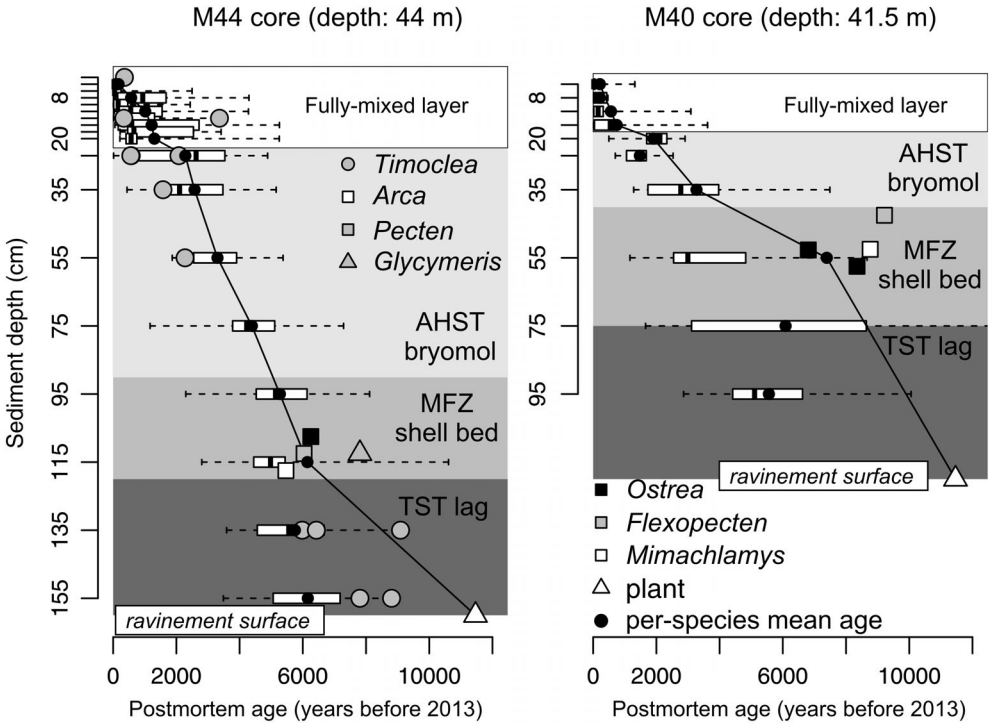

Fig. 3. Stratigraphic changes in age–frequency distributions of *Timoclea ovata* summarized by boxplots. Shown are millennial-scale time averaging, overlap between adjacent increments, and the slope of lines (a function of long-term sedimentation rate) connected by mean age estimates of individual increments. Boxplots are delimited by the 25th and 75th age percentiles and their width thus corresponds to time averaging (inter-quartile age range) of bivalve assemblages. The final age model is represented by black circles connected by solid lines. *Timoclea ovata* ages from increments below the MFZ interval are affected by the bioturbation-abundance effect and are excluded from the final age model. For abbreviations, see caption for Fig. 2.

Waltham, MA, USA). Here, new geochronological data from M40 and taphonomic data for two bivalves (*Timoclea ovata* and *Varicorbula gibba*) from M44 and M40 are presented. These are the focal cores in this study's analyses; the other two cores constrain the spatial variability in the deposition.

Schnedl *et al.* (2018) presented amino acid racemization (AAR) data with concentrations and D/L values of aspartic acid for 300 valves of *T. ovata* from 13 increments at M44, ^{14}C ages of 13 specimens of *T. ovata*, and ^{14}C ages of four other bivalve specimens. New AAR data for 118 valves of *T. ovata* from ten increments of M40 (Table S1) and ^{14}C ages of four bivalves (Table S2) from M40 were added; these were prepared with the same procedure as in Schnedl *et al.* (2018). The postmortem age of *T. ovata* is calibrated on the basis of the AAR-^{14}C relationship (Allen *et al.*, 2013) and is estimated with D/L of aspartic acid (Schnedl *et al.*, 2018). Ages were set relative to the year of collection (2013 AD = year zero). The age model used in this study is based on 426 valves of *T. ovata* from M40 and M44, on ^{14}C ages of eight additional bivalves (one *Arca, Glycymeris, Ostrea* and *Pecten* from M44, two oysters, one *Mimachlamys* and one *Flexopecten* from M40), and on the ^{14}C age of one terrestrial plant specimen (Table S3).

Skeletal alteration

Timoclea ovata and *Varicorbula gibba* are small-sized (<15 mm in length), aragonitic, shallow-infaunal, suspension-feeding bivalves that inhabit the uppermost few centimetres close to the sediment–water interface (SWI; Holmes & Miller, 2006; Morton, 2009). All specimens of these two species (complete valves or fragments with umbo preserved) were extracted from cores M44 and M40, counted and scored for alteration. Taphonomic scoring is divided into two parts. First, dated valves of *T. ovata* (n = 300 for M44 and n = 118 for M40; Table S1, Appendix S1)

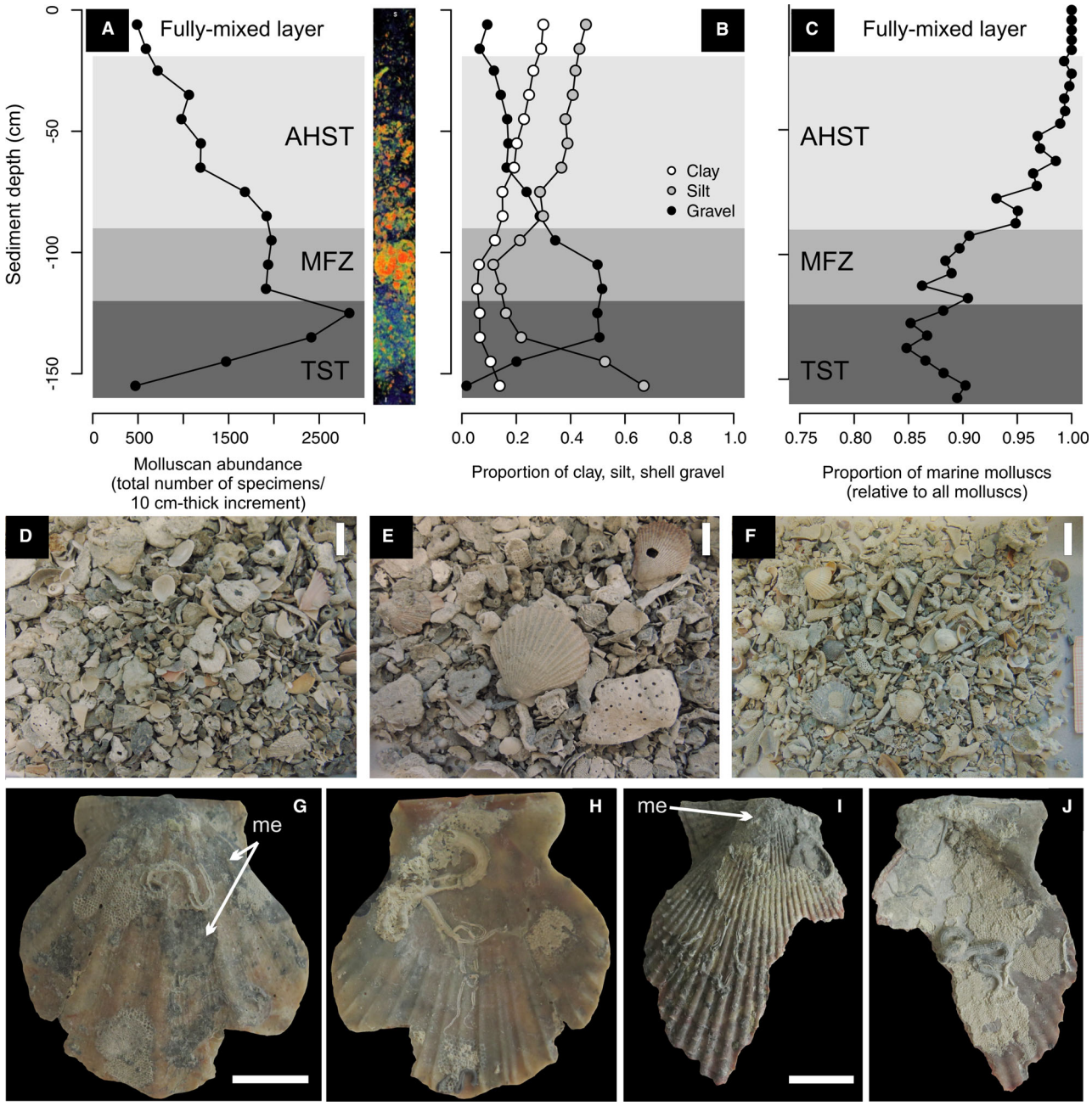

Fig. 4. (A) and (B) The upcore decline in two indices of shell abundance at M44, including total molluscan abundance in 10 cm thick increments [(A) with X-radiograph showing two shell beds in the TST and MFZ units; the lighter colours represent more dense carbonate particles, mainly sand-sized and gravel-sized remains of molluscs and bryozoans] and the proportion of shell gravel (B). (C) The upcore decline in the proportion of non-marine molluscan individuals at M44. (D) to (F) Residues of death assemblages sieved at 1 mm at M46, showing molluscan lag concentrations with stained bioclasts in the TST (D), the molluscan gravel in the MFZ shell bed (E) and bryomol with non-stained bioclasts in the AHST increments (F). (G) to (J) Scallops from the MFZ shell bed at M40 with encrusters and dark grey partial micrite rims and envelopes (me). (G) and (H) *Flexopecten glaber* dated with ^{14}C to 9123 calibrated years BP (45 to 50 cm). (I) to (J) *Mimachlamys varia* dated to 8701 calibrated years BP (50 to 55 cm). Scale bars: 1 cm.

were scored to assess the taphonomic clock at light-microscope magnification (20 to 50×). With the exception of ornamentation loss, these variables are scored as absent (0) or present (1). They include: (i) discolouration; (ii) external or internal encrustation (bryozoans, foraminifera, serpulids and coralline algae; also discriminate between well-preserved and worn encrusters); (iii) internal bioerosion (mainly *Entobia*); (iv) internal fine-scale dissolution (chalkiness and minor pitting); (v) intensely-worn surface with ornamentation loss (generated by intense dissolution or abrasion) with three categories (0 – absent, 0.5 – incomplete loss, 1 – complete loss); (vi) light grey penetrative staining that is patchy, with fuzzy boundaries, or penetrates through the whole, initially translucent or white valves; and (vii) cementation by micrite and microsparite, i.e. dark grey, discrete, irregular, millimetre-thick fine-grained cryptocrystalline crusts or fringes rimming valve surfaces and filling pores within valves. Such cementation is equivalent to micrite envelopes (Bathurst, 1966; Alexandersson, 1972a; Reid & Macintyre, 1998; Perry, 1999; Ge *et al.*, 2020a). Analyses at higher magnifications (500 to 1000×) show that these envelopes correspond to an interstitially-precipitated framework of granular or subhedral microcrystals (Deville de Periere *et al.*, 2011; Kaczmarek *et al.*, 2015) and to micritic or microspartitic epitaxial fringes lining skeletal pores (Reid *et al.*, 1990). They are also associated with incipient recrystallization of valves characterized by Sr enrichment localized around microborings.

Second, *all* valves of *T. ovata* ($n = 4174$ for M44 and $n = 1418$ for M40) and *V. gibba* ($n = 768$ for M44 and $n = 583$ for M40) were scored to assess stratigraphic changes in the frequency of five alteration types in increments pooled to 10 cm thick intervals. These types include: (i) frequency of external encrustation; (ii) frequency of worn valves (with ornamentation loss); (iii) frequency of stained valves or valves cemented with micrite envelopes; (iv) frequency of worn encrusters on encrusted valves; and (v) frequency of non-stained or non-cemented encrusters on stained or cemented valves (composite alteration). These variables were selected to separate processes at the SWI (encrustation) from subsurface (staining, cementation by micrite envelopes) and composite processes (stained or cemented valves exhumed to the SWI and then recolonized by encrusters).

The chemical composition of stained valves and valves cemented by micrite envelopes was analyzed in longitudinal thin sections of four *T. ovata* and three *V. gibba* valves with wavelength-dispersive spectroscopy and backscattered electrons (BSE), using a Jeol JXA-8530F electron probe microanalyzer (accelerating voltage: 15 kV; probe current: 15 nA; beam diameter: 5 to 10 μm; JEOL Ltd. Tokyo, Japan). The standards used in analyses (detection limits in ppm in parentheses) were diopside for Ca (335) and Mg (140), hematite for Fe (125), rhodonite for Mn (135), celestite for Sr (255) and barite for S (95).

Long-term sedimentation rate, time averaging and disintegration rate

Long-term sedimentation rate is estimated as the thickness of sediments bounded by dated intervals divided by the temporal distance separating those intervals (black circles connected by lines in Fig. 3; Table S3). *Time averaging* of assemblages in 5 cm increments is computed as an inter-quartile age range (IQR) based on all dated valves. The *raw* IQR is biased towards larger values by age errors induced by AAR-^{14}C calibration (Yanes *et al.*, 2007; Dominguez *et al.*, 2016). This bias is expected to produce an apparent downcore increase in time averaging even when there is none. This bias was accounted for in two ways. First, stratigraphic changes in raw IQR were assessed because a downcore constancy in raw IQR indicates that time averaging of older increments does not exceed time averaging of younger increments. Second, the error component as implemented in Tomašových *et al.* (2019a,b) was computed. This error component is subtracted from the raw IQR, producing an *error-corrected* IQR for which increments with an error component exceeding *ca* 1000 years are excluded. The IQR of ages of sedimentary particles expected under long-term sedimentation rate is calculated with the thickness of the fully-mixed layer set to 20 cm. The distribution of ages of sedimentary particles in the mixed layer is expected to be exponential when the sedimentation rate is constant over the duration of time averaging and sediment particles are buried stochastically below the mixed layer. The IQR of this distribution can be approximated as the natural logarithm of three divided by the inverse of time to burial of particles below the 20 cm thick fully-mixed layer (time to burial is estimated on the basis of long-term sedimentation rate).

The *disintegration rate* of aragonitic valves in the fully-mixed layer was estimated by fitting age distributions to two types of disintegration models (pooling both cores to maximize the number

of dated valves, with $n = 101$). This approach enabled distinguishing between: (i) a model with temporally-constant skeletal disintegration; and (ii) a sequestration model with temporally-declining disintegration, allowing that old valves can be more durable than young valves (Tomašových *et al.*, 2014). The fit of distributions to these models is evaluated with the Akaike Information Criterion corrected for small sample size (AICc).

Taphonomic clock and rate of alteration

The postmortem age of altered valves is not a simple function of alteration rate in the mixed layer because it also depends on time to disintegration (in the mixed layer) and burial (below the mixed layer). Nonetheless, the median ages of altered valves in the mixed layer exposed to active input of freshly-dead shells provide first-order information on half-time to valve alteration (i.e. low median age indicates fast alteration). Here, fully-mixed, age-homogenized layer is located in the upper 20 cm, and the underlying 70 cm thick unit are affected by deeper but incomplete mixing; crustacean burrows can extend up to 90 cm in the northern Adriatic Sea, Pervesler & Hohenegger, 2006. In a first step, the timing of alteration based on the age distributions of altered *T. ovata* valves in the mixed layer (both in the upper 20 cm and in the upper 90 cm of cores) was evaluated. Second, the taphonomic clock was assessed at three scales to determine whether the variation in alteration, explained by postmortem age, increases when the dated valves of *T. ovata* are pooled into age cohorts or increment-specific assemblages. For the *individual-level taphonomic clock*, analysis of principal coordinates constrained by postmortem age (with Manhattan distances) was performed. This analysis maximized the separation of valves based on their alteration in the whole core, factoring out the effect of sediment depth (separately for each core). For the *cohort-level taphonomic clock*, valves were aggregated to 100-year cohorts (in valves <1000 years old) and to 500-year cohorts (in valves >1000 years old) and the Pearson correlation between the cohort age and the cohort-level relative frequency of altered valves in the mixed layer was assessed. The time needed to alter half of the valves can be estimated in cohort-level analyses by identifying age cohorts that consist of at least 50% of altered valves. The *assemblage-level taphonomic clock* refers to the relationship between time averaging (interquartile age range of valves) and the assemblage-level alteration at the scale of 10 cm increments, using Spearman rank correlation.

Stratigraphic variability in assemblage-level alteration

To assess stratigraphic trends in alteration at the level of 10 cm increments, the relative frequency of valves altered by five variables (external encrustation, ornamentation loss, staining, worn encrusters on worn valves and non-stained encrusters on stained or cemented valves) was used. Principal coordinate analyses (based on five alteration variables and Manhattan distances among increments) and permutational multivariate analysis of variance (PERMANOVA; Anderson & Walsh, 2013) were utilized to assess whether the subsets of systems tracts differ in alteration. All analyses were performed with R Core Team (2018).

RESULTS

Age model

The age model follows Schnedl *et al.* (2018) but is updated here for both cores as follows:

1 The median age of *T. ovata* increases gradually downcore to a gravelly shell bed (visible in X-ray in Fig. 4A) at 90 to 120 cm in M44 (median: *ca* 5000 years) and at 45 to 75 cm in M40 (median: *ca* 6000 years; white boxplots in Fig. 3).
2 The ^{14}C ages of large valves of oysters, scallops and *Glycymeris* indicate that the formation of shell gravel was initiated *ca* 7800 years ago for M44 and 9300 years ago for M40. In contrast, most *T. ovata* valves from the same shell bed are younger (median age *ca* 5000 years for M44 and *ca* 3000 years for M40).
3 The age of terrestrial plant remains on the bottom of the M40 core indicates that the paralic deposition terminated *ca* 11 350 years ago. This estimate is consistent with the onset of flooding of habitats at 30 to 40 m depth in the northern Adriatic Sea, which was dated to *ca* 11 300 to 11 500 years BP (Cattaneo & Trincardi, 1999; Asioli *et al.*, 2001; Pellegrini *et al.*, 2015; Bruno *et al.*, 2017; Brunović *et al.*, 2020).
4 Individuals of freshwater and brackish species contribute *ca* 10% to the total molluscan assemblage in the lowermost 60 cm of M44 (Fig. 4C).
5 The median ages of *T. ovata* in the increments below the gravelly shell bed are younger than the ages of oysters and scallops in the same

shell bed, indicating that they are biased by the bioturbation-abundance effect (Broecker *et al.*, 1988). This effect refers to a preferential downward mixing of valves from younger increments with initially high *T. ovata* abundance to increments with initially low *T. ovata* abundance. The age model thus excludes *T. ovata* ages in increments underlying the shell bed in both cores.

Core lithology

Cores were subdivided into four stratigraphic units that differ in age, grain size and abundance of carbonate components (Figs 3 to 5). Even when the mean ages of these four units gradually decline upcore, their age distributions overlap due to mixing by bioturbation. Thus, their overall age can be defined by their age range rather than by a single mean age estimate (Fig. 5). The X-ray in Fig. 4A shows gradational boundaries between the four units at the scale of several centimetres. The $CaCO_3$ content in the 63 μm fraction varies between 30% and 40% in the whole core at M44, although these values underestimate the total carbonate content because the X-ray shows dense packing of sandy and gravelly remains of molluscs, bryozoans and echinoderms (Fig. 4A). The lowermost, 25 to 35 cm thick unit is represented by well-sorted to moderately-sorted gravelly sands with low content of clay (<15%). At M44, M46 and M40, this unit exhibits a coarsening-up trend from molluscan muddy sands to molluscan sandy gravel. Molluscan sediments at M44 contain abundant stained fragments of epifaunal and shallow-infaunal bivalves, vegetation-associated gastropods, infaunal echinoids (*Echinocyamus*), crustacean fragments, and irregular, several centimetre-long micritic concretions (Fig. 4D). The coarsening-up trend terminates in a second unit, represented by a 25 to 30 cm thick distinct shell bed with 50% shell gravel (Fig. 4E) and a low clay content (<20%); the silt and clay content increases in the uppermost part. This shell bed occurs at the base of M43 where the coarsening-up trend is absent. The shell bed contains large oysters, scallops and *Glycymeris* valves, bored by sponges and encrusted by coralline algae, serpulids and bryozoans, and coated by micrite envelopes (Fig. 4G to J). This bed also contains diverse small-sized epifaunal and infaunal bivalves, epifaunal gastropods and echinoids. Oysters (*Ostrea* sp.) attain 30 to 50 mm in height, in contrast to small-sized individuals (<10 mm) in the underlying and overlying units. The per-increment height of the scallop *Mimachlamys varia* fluctuates between *ca* 5 mm and 15 to 20 mm in the underlying and overlying units but increases to 30 to 35 mm in the gravelly shell bed. The gravelly shell bed is overlain at all sites by the third, 30 to 80 cm thick bryomol unit with a fining-upward trend, with poorly-sorted bryozoan–molluscan muddy sands replaced by sandy muds (Fig. 4F). These increments consist of abundant bryozoans (*Cellaria* and *Pentapora*), mostly non-stained, infaunal and epifaunal molluscs and coralline algae. The fourth unit corresponds to the uppermost 16 to 20 cm, representing the age-homogenized, fully-mixed layer with uniform median per-increment shell ages (with the mixture of skeletal particles that are several centuries old and 20th century shells). It is formed by shell-poor sandy muds with dispersed bryozoans, infaunal molluscs and coralline algae. The per-increment age distributions of *T. ovata* in this unit are right-skewed, with modes formed by valves younger than 100 years in all increments (Fig. 5).

Systems tracts

Although the stratal geometry is difficult to estimate due to short distances between sediment cores and differential progradation that is typical of the northern Adriatic Sea may generate diachronous systems tracts (Madof *et al.*, 2016), these units are assigned to subsets of systems tracts based on Holocene changes in accommodation space inferred for Brijuni (Antonioli *et al.*, 2007) and on corresponding changes in sediment thickness as constrained by the age model. The maximum ingression documented on the Istrian peninsula took place *ca* 6000 years ago (Faivre *et al.*, 2011; Felja *et al.*, 2015), coinciding with a turnaround between retrogradation and progradation (at 5000 to 7000 years BP) in the north-western Adriatic Sea and in the Gulf of Trieste (Amorosi *et al.*, 2008, 2017; Zecchin *et al.*, 2015). The thickness of sediments deposited during the rapid sea-level rise prior to the maximum ingression (represented by the 25 to 35 cm thick lowermost unit with molluscan sands located above the wave-ravinement surface) indicates that the sediment supply significantly lagged relative to the newly-created accommodation space. This first unit can thus be assigned to the transgressive systems tract (TST). The increments in the second

unit (gravelly shell bed, *ca* 5000 to 8000 years BP) approximately coincide with the maximum ingression and can be assigned to the maximum flooding zone (MFZ). The bays and estuaries along the Istrian peninsula that were flooded during the maximum ingression were filled with prograding sediments during the latest Holocene (Faivre *et al.*, 2011; Felja *et al.*, 2015; Novak *et al.*, 2020a). Nonetheless, with the exception of bays, the shoreline along most of the Istrian peninsula did not prograde during the latest phase of sea-level stabilization owing to an extremely reduced fluvial sediment supply and sediment bypassing, and sediments deposited during the highstand phase are thus typically less than 1 m thick (Tomašových *et al.*, 2019b; Novak *et al.*, 2020b). The thickness of the bryomol unit overlying the gravelly shell bed at Brijuni approximately matches the vertical increase in the accommodation space as predicted by the relative sea-level rise estimated for Brijuni. This match indicates that the depositional system during the latest sea-level phase was in the aggradational mode. The bryomol unit is thus assigned to the aggradational, even when very thin, highstand systems tract (AHST; e.g. Zecchin *et al.*, 2006). The uppermost unit is treated separately because it is age-homogeneous and actively mixed.

Within-sequence changes in long-term sedimentation rate and in time averaging

The thickness of the TST unit is 50 cm at the shallowest site M40, is absent at M43, and is 30 to 40 cm at M44 and M46 (Fig. 2C). The MFZ shell bed slightly increases in thickness towards the shallowest site. The AHST unit is 70 to 80 cm thick at deeper sites, 50 cm thick at M43, and 30 cm thick at M40. Long-term sedimentation rates fluctuate from *ca* 0.01 to 0.03 cm year^{-1} (Fig. 5). The estimated time averaging of bivalve assemblages in 5 cm increments under these sedimentation rates and the 20 cm thick fully-mixed layer is predicted to vary from *ca* 500 to 1000 years in the AHST, *ca* 1000 to 1500 years in the MFZ shell bed at M44, *ca* 4000 years in the MFZ shell bed at M40 and *ca* 1000 to 3000 years in the TST unit (Fig. 5).

Subsurface age distributions below the fully-mixed layer are weakly-skewed or unskewed and are averaged to few millennia (Fig. 5). In contrast, the age distributions of 4 cm increments in the upper 20 cm in both cores are right-skewed, with multi-centennial averaging (raw IQR = 280 to 1800 years at M44 and 300 to 660 years at M40, error-corrected IQR = 240 to 1400 years at M44 and 140 to 430 years at M40). Assemblages at M44 are averaged to 1000 and 2000 years between 35 cm and 155 cm, and the maximum of 3000 years occurs in the AHST at 20 to 25 cm. Assemblages at M40 are averaged to 1900 years in the TST, to 4900 years in the MFZ shell bed, and to 2100 years in the AHST. Therefore, time averaging remains relatively constant at M44 and declines upcore at M40 (Fig. 5). When grouping the increments to four stratigraphic units, the median per-increment IQR is 1090 years in the TST, 3200 years in the MFZ, declining to 1570 years in the AHST and to 640 years in the fully-mixed layer. Error-corrected time averaging is 1100 to 2300 years at M44 and 1100 years at M40. Empirical time averaging based on bivalve ages in subsurface increments is comparable to time averaging predicted by long-term sedimentation rates (Fig. 5). In contrast, surface increments in the fully-mixed layer are less time-averaged than expected based on the long-term sedimentation rate.

Skeletal alteration

Timoclea ovata valves vary strongly in the degree and nature of alteration even within 10 cm increments. They include pristine valves without any modification (Fig. 6A and B), encrusted but otherwise pristine valves (Fig. 6C and D), and bored, worn and stained valves with encrusters (Fig. 6E to H). The latter are frequently covered by patchy dark-grey micrite that fills serpulid tubes (Fig. 6G and H), bryozoan zooids and cell compartments in algae (Fig. 6I to J). This micrite also covers spaces between ribs (Fig. 6K). Worn and stained valves are also encrusted by well-preserved encrusters (Fig. 6L). *Varicorbula gibba* is represented by well-preserved valves (Fig. 6M and N), by worn and non-stained valves with encrusters (Fig. 6O and P), and by worn and stained valves with worn encrusters and micrite envelopes (Fig. 6Q to X). Thin sections of *T. ovata* and *V. gibba* show that pristine valves characterized by smooth internal surfaces exhibit original colour and do not show staining or micrite envelopes (Fig. 7A and E). Borings in encrusted valves lacking micrite envelopes remain empty (Fig. 7B), whereas other encrusted valves are stained and covered by incomplete micrite envelopes (Fig. 7C, D and K), with borings also filled by micrite or microsparite (Fig. 7F to G, L to M). The surfaces of stained and cemented valves are worn.

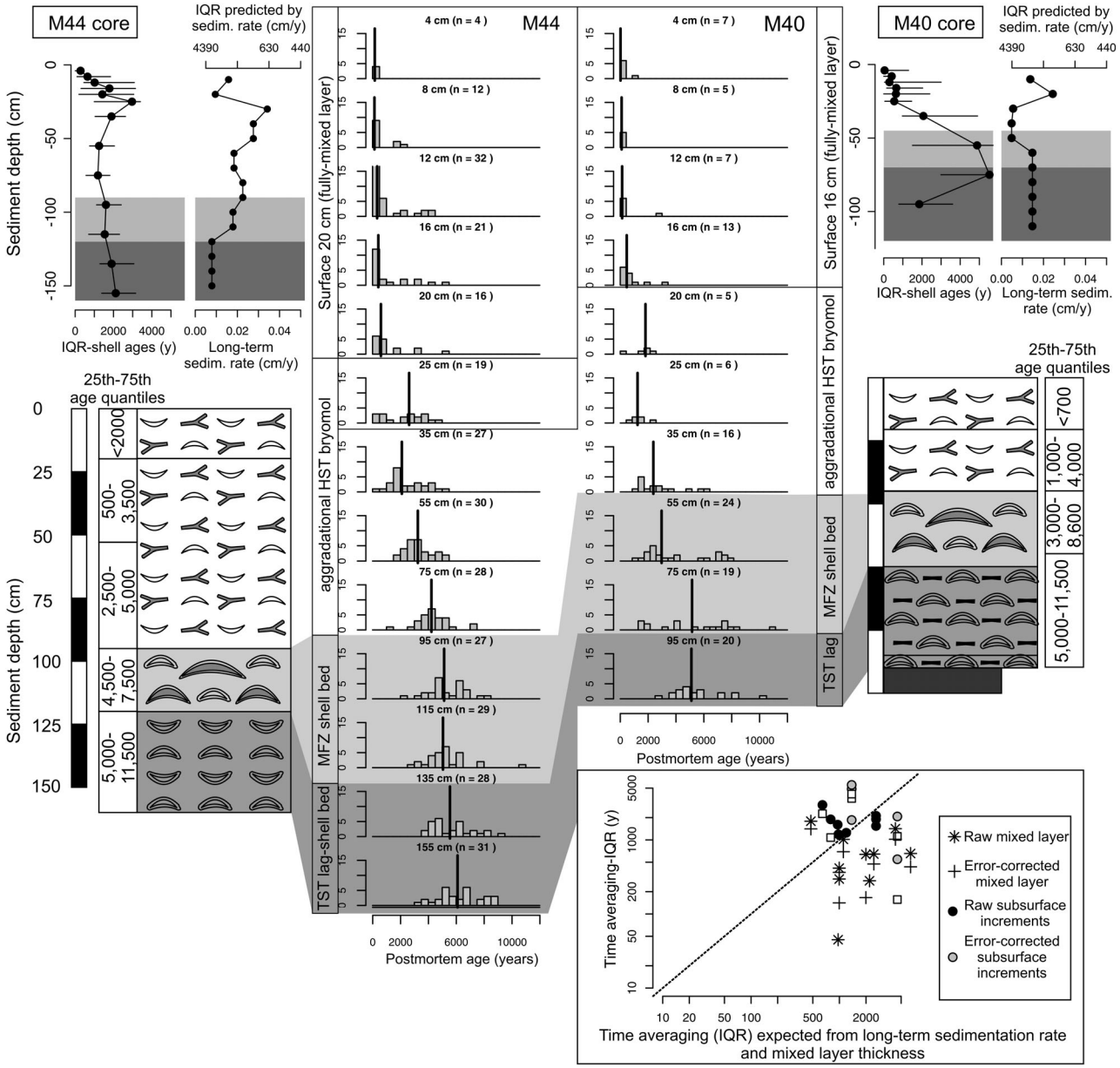

Fig. 5. The age distributions of bivalves stratigraphically shift from normal-shaped distributions in subsurface increments to right-skewed distributions in the fully mixed layer. Age ranges assigned to individual stratigraphic units correspond to the 25th and 75th quantiles of age distributions. Top insets: minor stratigraphic variability in time averaging (IQR of valve postmortem ages) and in long-term sedimentation rate. The bottom inset on the right shows that time averaging computed from the long-term sedimentation rate (here fluctuating between *ca* 0.01 and 0.03 cm year^{-1}) and the depth of the fully mixed layer (*ca* 20 cm) is congruent with the scale of time averaging computed from dated valves in 5 cm subsurface increments. Increments in the mixed layer are less time-averaged than expected based on the long-term sedimentation rate.

Micrite-sized crystals contribute to envelopes and cementation in intraskeletal pores within valves or in pores among valves in three forms. First, granular or clustered aggregates of randomly-arranged, globular or subhedral, fully or incompletely fused microcrystals of variable size (1 to 5 μm, Fig. 7N) form irregular, incomplete envelopes around valve surfaces (Fig. 8A

to D). They are also located in pores and borings >5 to 10 μm in diameter (Fig. 8C and D) and fill the conchiolin layer of *V. gibba* (Fig. 8H and I). The framework formed by these aggregates is typically porous, binds other larger loosely or densely packed sedimentary grains, and embeds clay flakes and pyritic grains (Fig. 8E). Second, epitaxial isopachous fringes of dentate crystals line borings within valves and intraskeletal voids of encrusting coralline algae, bryozoans and serpulids (Fig. 8F). They are mostly shorter than 5 μm but can develop into larger microspar (*ca* 10 μm). These two types – the framework of microcrystals and the epitaxial micrite or microspar [both dark grey in back-scatter electron images (BSE)] – are formed by high-Mg calcite and represent the volumetrically most important cements. They are consistently rich in Mg (*ca* 10 to 13% mol $MgCO_3$) and S (>1500 ppm) and poor in Fe (<1000 ppm). Third, an irregular mesh with acicular aragonite needles (mostly shorter than 5 μm, locally up to 10 μm) can line borings and pores (Fig. 8G and H). In some borings, thin acicular fringes <1 μm of aragonite form the earliest fringes that are succeeded by coarser crystals of high-Mg calcite.

Magnesium concentrations detected in valves of *T. ovata* and *V. gibba* are consistently low (<200 ppm). Sr concentrations attain 1700 to 1800 ppm in *T. ovata* and 1100 to 1500 ppm in *V. gibba*. S and Fe in stained valves are enriched in zones with intense bioerosion, forming a halo around the high-Mg calcitic infill of the conchiolin layer (Fig. 8H and I). BSE images show that this enrichment is triggered by nanopyritic inclusions (<1 to 2 μm) that fill small microborings and fractures (1 to 2 μm in diameter; Fig. 8M to O; comparable to nanopyrite in echinoderm ossicles in Brand & Morrison, 1987). In addition, the external margins of valves cemented by micrite or microsparite are characterized by *ca* 50 μm thick recrystallized (light-grey colours in BSE) non-pyritic zones around larger microborings (>5 to 10 μm in diameter). These zones are enriched in Sr (2100 to 2600 ppm in *V. gibba*).

Individual-level and cohort-level taphonomic clock

Postmortem age–frequency distributions of valves altered in the mixed layer show two distinct types. In the fully-mixed layer, valves with bioerosion, dissolution and well-preserved encrusters are typically young (minimum age – few decades, median age *ca* 500 years). In contrast, valves with worn encrusters, ornamentation loss, staining and micrite envelopes are on average older (median age = 1000 to 2000 years, Fig. 9A and B). Extending the thickness of sediments to the upper 90 cm, age distributions of *T. ovata* valves altered by bioerosion, fine-scale dissolution and encrustation are bimodal (Fig. 9C and D). The first mode is formed by young valves (<500 years old), the second by old valves (*ca* 2000 to 4000 years old). In contrast, valves affected by ornamentation loss, staining and micrite envelopes are rarely younger than 1000 years and mostly older than 2000 years (Fig. 9D). The minimum age of stained valves and valves cemented by micrite envelopes is 360 years at M44 and 430 years at M40.

Constrained analyses of principal coordinates show that less than 10% of the variation in alteration is explained by postmortem age of valves in *T. ovata* when the effect of sediment depth is factored out [F (M44) = 10.9, $P < 0.001$, $R^2 = 0.07$, F (M40) = 3.3, $P = 0.011$, $R^2 = 0.06$]. However, the amount of variation explained by postmortem age in this species increases to 85% (staining), 82% (micrite envelopes) and 65% (ornamentation loss) at M44 and to 72% (micrite envelopes) and 73% (ornamentation loss) at M40 when valves are aggregated to 100 and 500 year cohorts (Fig. 10; Table S4). Bioerosion and fine-scale dissolution occur at the highest rate: their frequency increases to >50% within the first 500 years (Fig. 10A and B). Encrustation is also fast because it increases to 40 to 50% within the first 500 years. In contrast, well-preserved encrusters decline in frequency with increasing age because they deteriorate, and encrusters on older valves are frequently worn. Ornamentation is worn in 15 to 30% of valves that are 500 years old, and its frequency gradually increases to *ca* 50 to 60% in valves older than 2000 years (Fig. 10C and D). Staining and the precipitation of micrite envelopes occur at the slowest rate because their frequency increases above 20% after *ca* 2000 years and *ca* 50% of valves are stained or cemented after *ca* 5000 years (Fig. 10E and F).

Assemblage-level taphonomic clock

Per-increment frequencies of bored valves correlate positively with frequencies of encrusted valves. Per-increment frequencies of stained valves also correlate positively with frequencies

of valves with micrite envelopes (Fig. 10). The relations between frequencies of encrusted and bored valves on one hand and frequencies of stained valves and valves with micrite envelopes on the other hand are more complex. Most stained valves and valves with micrite envelopes are bored and encrusted, whereas many bored and encrusted valves remain unaffected by staining or micrite envelopes (Fig. 11). The frequencies of worn valves covary positively with all other types of alteration (Fig. 11). Despite this complexity, time averaging (raw IQR) correlates positively with the frequency of valves altered by encrustation, bioerosion, ornamentation loss, staining and micrite envelopes (Spearman $r = 0.39$ to 0.62; Fig. 11; Table S5). The increments with more than 50% of worn valves and with at least 25% of stained valves and valves with micrite envelopes are averaged to more than 2000 years. Alteration frequencies thus discriminate between increments with multi-centennial time averaging and increments with millennial time averaging.

Within-sequence decline in alteration

Even when net sedimentation rates and time averaging do not discriminate between systems tracts, assemblage-level alteration declines upcore and differs between TST, MFZ and AHST in both cores (Fig. 12). In *V. gibba*, stained valves, valves with micrite envelope and with composite alteration are most frequent in the TST unit and decrease upward. In *T. ovata*, encrusted valves, encrusted valves with worn encrusters and valves with composite alteration also decrease in frequency upcore. Worn, stained and cemented *T. ovata* valves are most frequent in the MFZ shell bed (Fig. 12), whereas *V. gibba* valves are more frequently worn, stained and cemented than those of *T. ovata* in the TST unit (Fig. 12). Regardless of these interspecific differences, more than 50% of valves are stained and exhibit micrite envelopes in the TST and MFZ units. Increment-level principal coordinate analyses and PERMANOVA support differences in alteration levels between systems tracts [Fig. 13, F (*T. ovata*) = 11.1, $P < 0.001$, $R^2 = 0.6$, F (*V. gibba*) = 17.4, $P < 0.001$, $R^2 = 0.7$].

DISCUSSION

Subsurface origin of micrite envelopes and staining by pyrite

Encrustation of infaunal bivalves by coralline algae, serpulids, bryozoans or foraminifera, and their bioerosion by sponges and other boring organisms, require that the remains of such bivalves resided at the sediment–water interface (SWI) in the uppermost levels of the mixed layer. Median times to bioerosion and encrustation indicate that these processes occur rapidly at decadal scales. The upper zones of the mixed layer that are irrigated by oxic waters and exposed to aerobic degradation of organic matter and to H_2S oxidation can also contribute to disintegration by inducing carbonate dissolution (Walter *et al.*, 1993; Hu & Burdige, 2008). Fine-scale dissolution probably occurs in such zones close to the SWI because the median time to dissolution of valves in the upper 20 cm (Fig. 9A and B) is comparable to that of encrustation and bioerosion. Pore-water profiles of carbonate-rich sediments in the north-eastern Adriatic Sea tend

Fig. 6. Alteration of *T. ovata* (A) to (L) and *V. gibba* (M) to (X). (A) to (B) Pristine valve. M44-90-95-3 (6060 years). (C) to (D) Pristine valve with well-preserved external (coralline algae) and internal encrusters (bryozoans). M44-90-95-12 (7520 years). (E) to (F) Stained valve with worn ornamentation and well-preserved bryozoans on the exterior. M44-150-155-1 (6100 years). (G) and (H) Stained valve with micrite envelopes (me), stained serpulids and non-stained foraminifera. M44-110-115-14. (I) and (J) Stained valve with micrite envelopes (me) and stained bryozoans. M44-130-135-18. (K) Stained valve with micrite between ribs (me). M44-70-75-9 (9900 years). (L) Stained valve with well-preserved encrusters. M44-50-55-7 (3280 years). (M) and (N) Pristine valve. M40-20-25 cm. (O) and (P) Encrusted and non-stained valve with ornamentation preserved, M40-50-55 cm. (Q) and (R) Worn and stained valve with stained encrusters, M40-80-85 cm. (S) and (T) Stained valve with coralline algae filled with micrite cement (me) and non-stained serpulids, M40-50-55 cm. (U) and (V) Stained valve with grey (stained) serpulids and white (non-stained) coralline algae. M40-30-35 cm. (W) Worn and stained valve with white (non-stained) dendritic agglutinated foraminifera, M40-70-75 cm. (X) Stained valve with stained and non-stained encrusters and dark micrite envelopes (me). M40-75-80 cm. Scale bar: 2 mm.

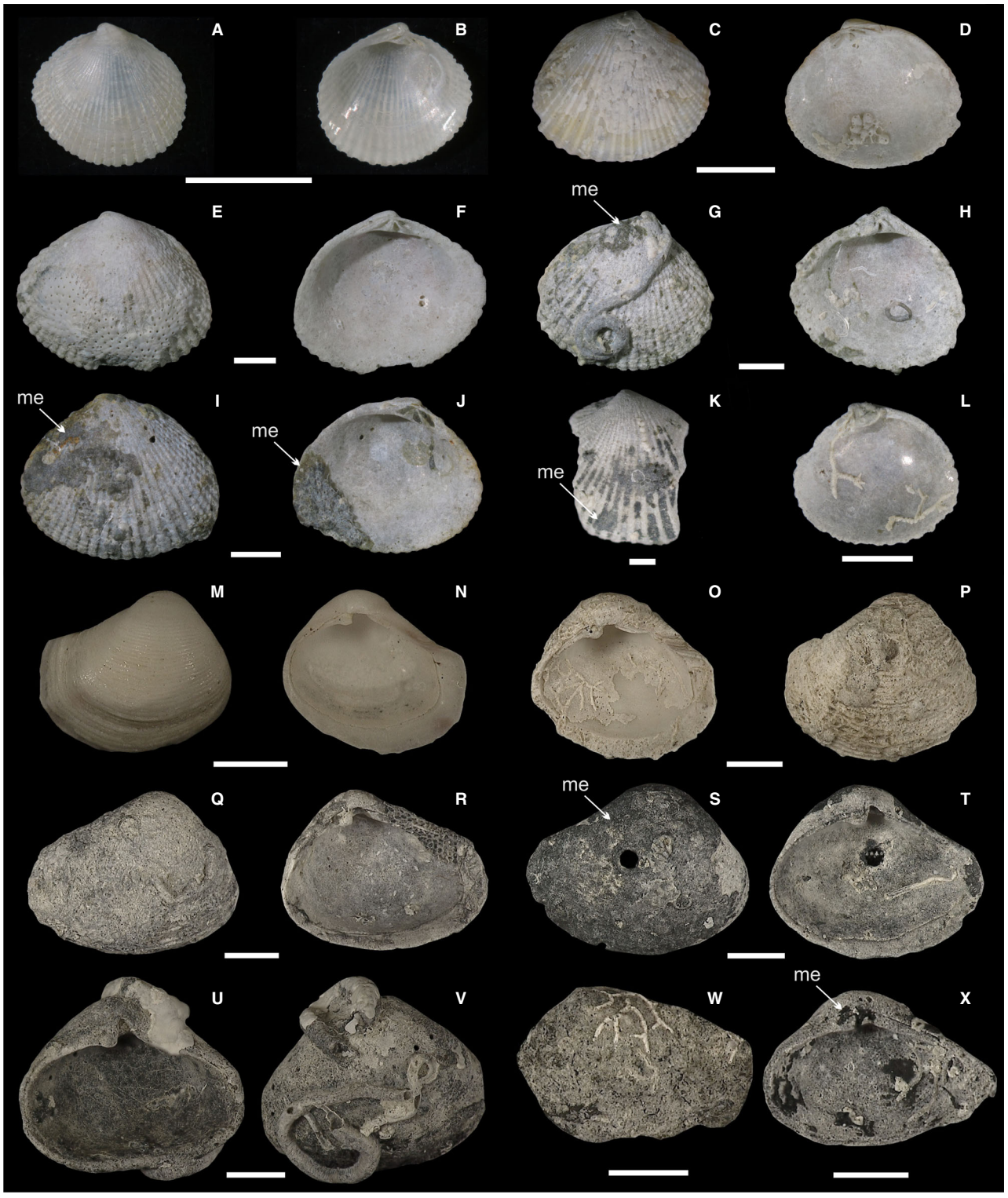

to show undersaturation with respect to aragonite in the upper 20 cm of sediments (Ogrinc & Faganeli, 2003). These well-mixed upper 20 cm are thus assigned to the TAZ.

In contrast to these alteration processes close to the SWI, several lines of evidence indicate that staining and micrite and microspar precipitation occur under permanently reducing conditions

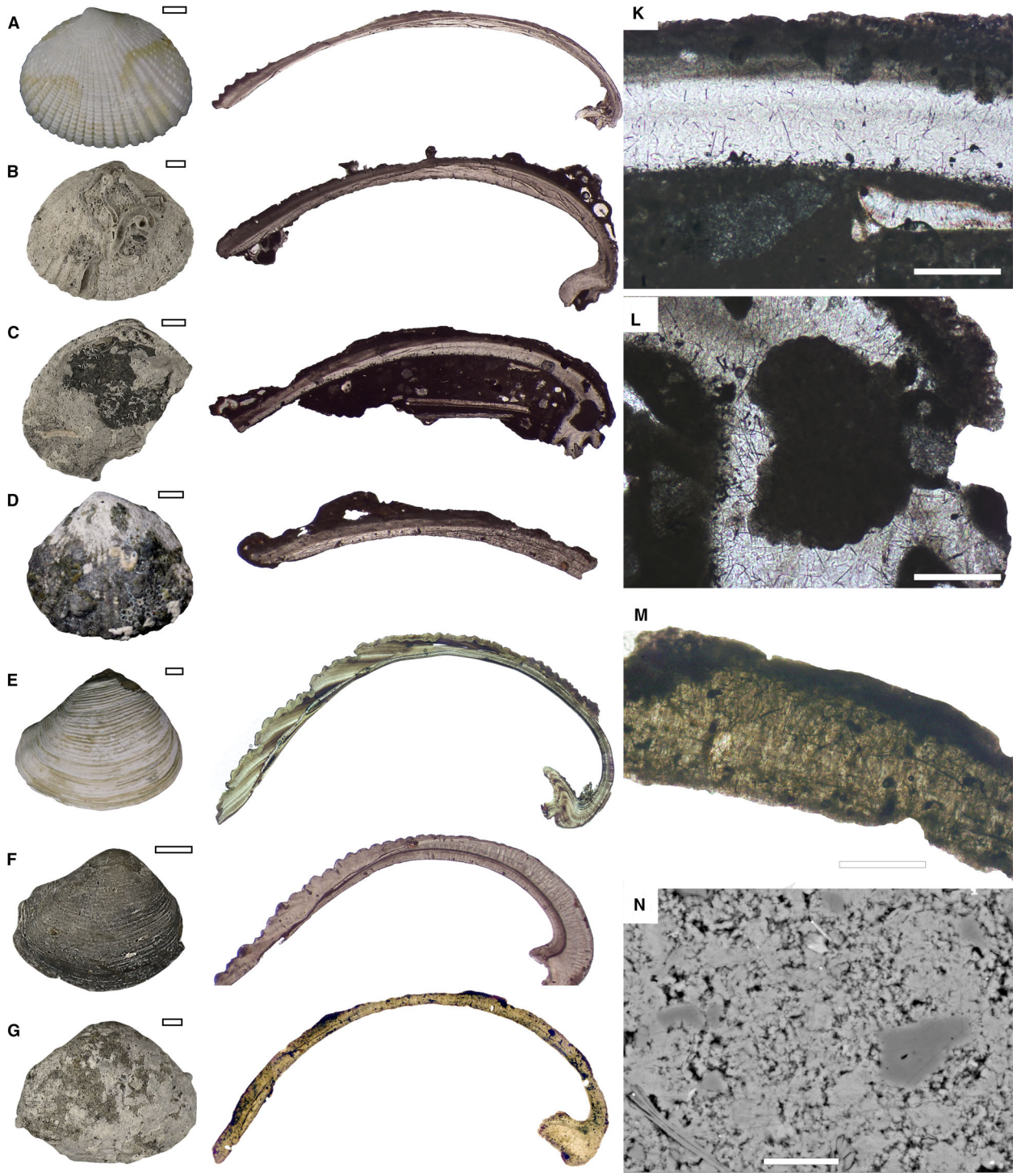

Fig. 7. Thin sections showing a progression in alteration from pristine towards worn, stained and cemented valves of *T. ovata* (A) to (D) and *V. gibba* (E) to (G). (A) Pristine valve (M44-130-135cm-32). (B) Encrusted and bored valve without staining and cements (M40-75-80cm-2). (C) Encrusted, bored and stained valve with micrite envelopes (M40-75-80cm-3). (D) Encrusted valve with worn ribs, coralline algae and micrite envelopes (M44-130-135cm-17). (E) Pristine valve (M13-65-70cm-29). (F) Bored and stained valve with micrite infills (M44-140-145 cm-5). (G) Bored and stained valve with micrite infills and worn encrusters (M44-140-145cm-2). (K) and (L) Micrite envelopes in *T. ovata* in (C). (M) Dense sponge borings filled by micrite in *V. gibba* in (G). (N) Backscattered electron image of a porous micrite with variable size (1 to 5 μm) and variable degree of coalescence, with floating clastic grains in a boring in *T. ovata* in (C). Scale: 1 mm in (A) to (G), 200 μm in (K) to (M) and 10 μm in (N).

below the fully-mixed layer at depths >20 cm, i.e. in the sequestration zone (SZ; but within reach of deeper burrowers and physical mixing; Fig. 14). First, the exclusive occurrence of nanopyritic inclusions in micron-scale borings in stained valves and their absence in non-stained valves demonstrate that these valves were stained in reducing zones with sulphate reduction. Second, valves in the upper 20 cm that are stained and cemented by micrite envelopes are on average older than 1000 years. Valves that are 1000 to 3000 years old are, however, most common in increments at 20 to 50 cm in both cores (Fig. 5). Therefore, these old valves were stained and cemented at depths >20 cm within the SZ and were later exhumed into the TAZ. Third, the micrite cements clearly precipitated in subsurface conditions (in interstitial cavities among valves) in the TST and MFZ units because they fill microporosity and bind bioclasts on external and internal valve surfaces. Fourth, staining and micrite precipitation probably formed simultaneously because they positively covary at the scale of individual increments (Fig. 11) and age distributions of stained and cemented valves are similar (Fig. 9). Moreover, stained portions of valves, typically in intensely microbored zones, form haloes around internal or external cements (Fig. 8J to L). The pyrite is interspersed within the interstitial micrite framework and the concentrations of iron in sediments at Brijuni are relatively low (1 to 2 wt.% throughout the core; Schnedl *et al.*, 2018). Accordingly, the non-ferroan micrite probably precipitated in reducing conditions within the SZ where bioirrigation is rare. In these zones, long-lasting sulphate reduction (associated with pyrite precipitation) or anaerobic methane oxidation increase the $CaCO_3$ saturation state (Raiswell, 1988, Baumgartner *et al.*, 2006; Capozzi *et al.*, 2012; Gallagher *et al.*, 2012; Taviani *et al.*, 2015; Meister *et al.*, 2018; Ge *et al.*, 2020b; Zhang, 2020) and carbonate ions sourced by the dissolution of aragonitic and high Mg-calcitic remains in the TAZ can accumulate by downward diffusion (e.g. Jenkyns, 1974; Munnecke & Samtleben, 1996). This conclusion is supported by the positive correlation between the frequencies of worn (intensely-dissolved) valves and stained and cemented valves (Fig. 11). They both peak in the TST and MFZ units (Figs 11F, 11G and 12), indicating close proximity of dissolution and cementation. Temporal variability in the irrigation depth of burrowers, with oxygenated pore waters locally penetrating into the SZ, can probably also generate transient dissolution and cement precipitation at similar sediment depths, with micrite precipitating in reducing microniches (Clari & Martire, 1996; Sanders, 2001; Zhu *et al.*, 2006).

Timescale of alteration and residence times in the taphonomic active zone and sequestration zone

The age distributions of altered valves and the dependence of assemblage-level alteration on post-mortem age document differences in the time needed to alter a high proportion of bivalves in the mixed layer (Figs 9 and 10). On one hand, the abundant young valves affected by bioerosion, encrustation and fine-scale dissolution indicate that these processes occur at high rate: valves in the TAZ are lost at a mere decadal or centennial-scale. On the other hand, the rarity of very young stained and cemented valves and their higher abundance in cohorts older than 2000 years indicate slow staining and micrite precipitation (Figs 9 and 10). Accordingly, high frequencies of stained valves and valves with micrite envelopes document their millennial-scale residence time in the SZ. This inference agrees with observations that high frequencies of stained and cemented skeletal particles are typical of sediment-starved environments in the Mediterranean (Corselli *et al.*, 1994; Toscano & Sorgente, 2002; Brandano & Civitelli, 2007). Nonetheless, it is suggested that these processes initially occur in subsurface sediment zones and depend on reducing pore-water conditions.

The timescale of staining and micrite precipitation is determined not only by the timing of burial into the SZ and by pore-water chemistry in the SZ but also by the initial priming of valves in the TAZ. This is because: (i) nanopyrite occurs in micron-scale microborings or dissolution pits; and (ii) micrite precipitates in larger borings and pores. Staining and micrite precipitation thus depend on valve microporosity that is typically generated by destructive processes in the TAZ. Importantly, bioerosion and dissolution tend to be fast in the TAZ. Accordingly, the accrual of staining and micrite cements is probably ultimately governed by a long residence time of valves in subsurface zones exposed to anaerobic degradation of organic matter and to the import of carbonate ions from dissolved valves in the TAZ (with a minimum of several hundreds of years as indicated by the youngest stained and cemented valves). Millennial scales of micrite precipitation are congruent with former estimates of

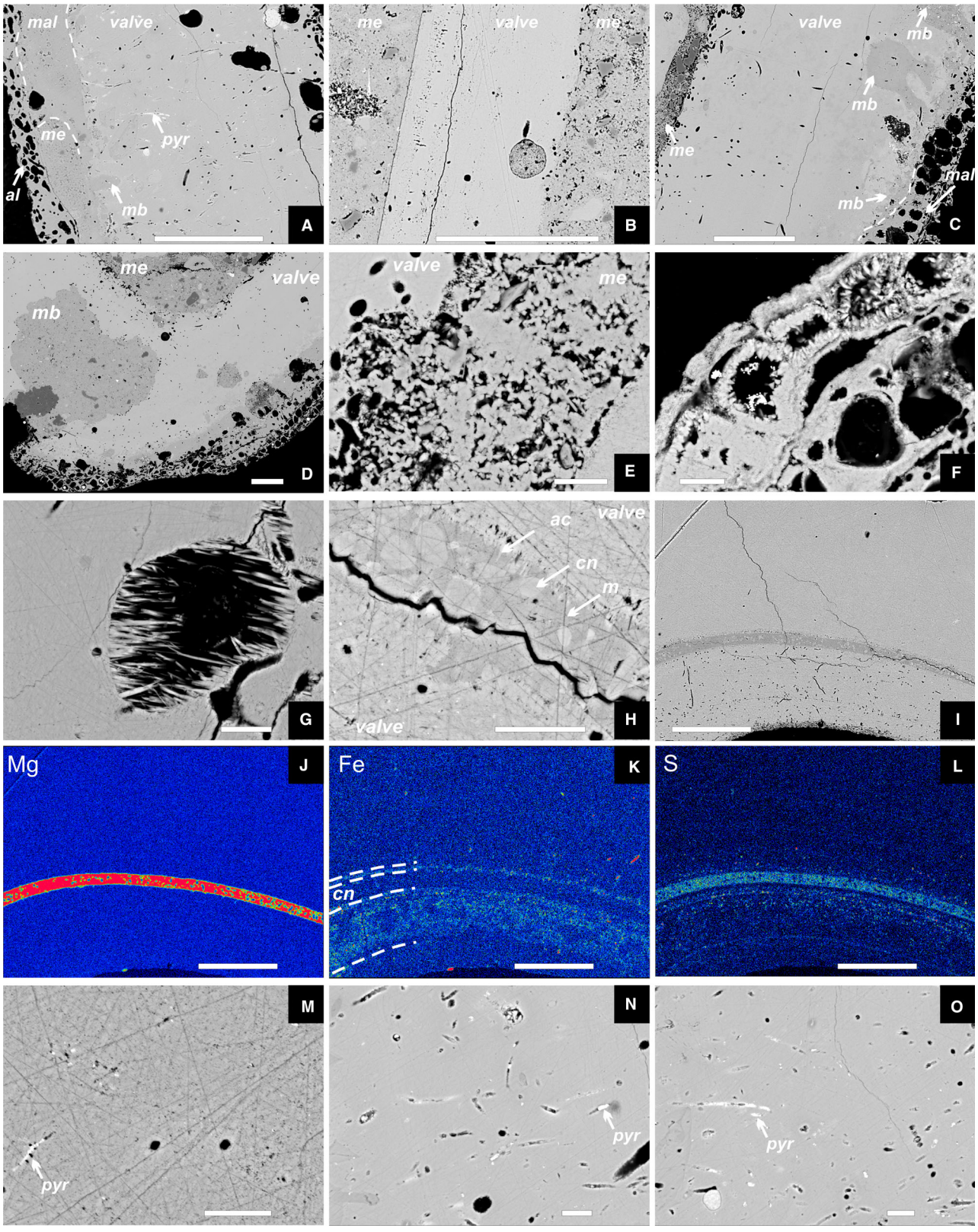

Fig. 8. Backscattered electron images and element maps of stained and cemented valves. (A) Bored and stained *V. gibba* with pyritic crystals (pyr) in borings and with a micrite envelope on the left (dark grey) with micrite-filled borings (mb), porous micrite (me) and coralline algae filled by epitaxial cements (mal) and empty voids (al), M44-140-145cm-2). (B) *T. ovata* rimmed by a porous micrite (me) on both sides (M40-75-80cm-2). (C) and (D) *T. ovata* with micrite in sponge borings (mb), coralline algae partly filled by micrite cement (mal) and porous micrite on the internal side (me). (E) Micrite grains interspersed with other small grains in the envelope that rims the interior of *T. ovata*. (F) Dentate crystals of high Mg-calcite lining cell compartments of coralline algae on *T. ovata*. (G) Acicular aragonite lining the boring in *T. ovata*. (H) The conchiolin layer of *V. gibba*, with micron-scale acicular cements lining the former pore space (ac), light-grey aragonitic nodules (cn), and darker high-Mg calcitic cement (m). (I) The conchiolin layer filled by cement and carbonate nodules, with intensely microbored inner layer located below it (M44-140-145cm-5). (J) to (L) The corresponding element maps show high-Mg calcitic cement within the conchiolin layer (cn) and the halo-forming enrichment around the conchiolin layer by iron and sulphur (dashed lines delimit the inner and outer halo). The conchiolin layer is also enriched in sulphur owing to the presence of pyrite. (M) to (O) Inclusions of nanopyrite that fill microborings in stained valves of *V. gibba*. Scale bars in (A) to (C), (I) to (L): 100 μm, all other scale bars: 10 μm.

micrite precipitation in intra-skeletal pores in the Mediterranean Sea (Alexandersson, 1972b). Although the rate of high Mg-calcite cement precipitation can markedly vary across marine environments not affected by meteoric diagenesis (Milliman & Müller, 1973; Allouc, 1990; Christ *et al.*, 2015), the relation between postmortem age and frequency of valves cemented with micrite indicates that a residence time of >1000 years in the SZ can be needed to cement a high proportion of valves in non-tropical environments (e.g. Nelson & James, 2000; Michel *et al.*, 2019) comparable to those at Brijuni.

Composite alteration documents burial/exhumation cycles

Valve alteration in the subsurface stratigraphic record is influenced by three processes: (i) their disintegration rate in the TAZ; (ii) the burial rate (from the TAZ to the SZ, and from the SZ to the FZB, when valves enter the final stratigraphic record); and (iii) by the exhumation rate from the SZ to the TAZ, which determines their residence time in the TAZ and SZ (Fig. 14). These transitions are inherently stochastic and driven by patchiness in mixing and bioirrigation. They can also reflect rapid erosional or burial events that randomize locations of sedimentary particles relative to the SWI. The variability in O_2 sediment penetration and H_2S oxidation does not translate to a simple depth that separates oxic from anoxic pore waters (Aller, 1994). Nonetheless, the base of the fully-mixed layer is simplified here to an average depth boundary between the TAZ (in the upper 20 cm, dominated by destructive processes) and the SZ (dominated by staining and cementation). The lower boundary of the SZ with sulphate reduction and micrite precipitation is difficult to constrain. However, the total organic carbon (TOC) concentrations decline from 1.6 to 1.1% dry weight in the upper 50 cm and remain between 1 to 1.1% downcore (Schnedl *et al.*, 2018). The presence of old but well-preserved valves unaffected by staining or cements at depths >50 to 100 cm can indicate that such valves were buried by burrowers even below the SZ. The preservation of such valves at high depths means that the SZ zone with cementation and staining is not more than a few decimetres thick and does not extend to the bottom of the cores.

The transitions of valves between the TAZ and the SZ ultimately influence the ability of the taphonomic clock to track hiatus duration. Such transitions determine whether the skeletal particles disintegrate quickly in the TAZ or are strengthened by micritic cements in the SZ. Individual valves ultimately preserved in the historical layer probably followed seven basic pathways through these zones:

1 Pristine and non-stained valves indicate rapid burial (by burrowers or by addition of new sediment) below the TAZ and below the SZ.
2 Encrusted and bored but non-stained or non-cemented valves indicate that omission in the TAZ was followed by rapid burial below the SZ.
3 Valves that were not buried in the SZ or that were rapidly exhumed back from the SZ to the TAZ are altered and disintegrate in the TAZ. Therefore, worn but non-stained or non-

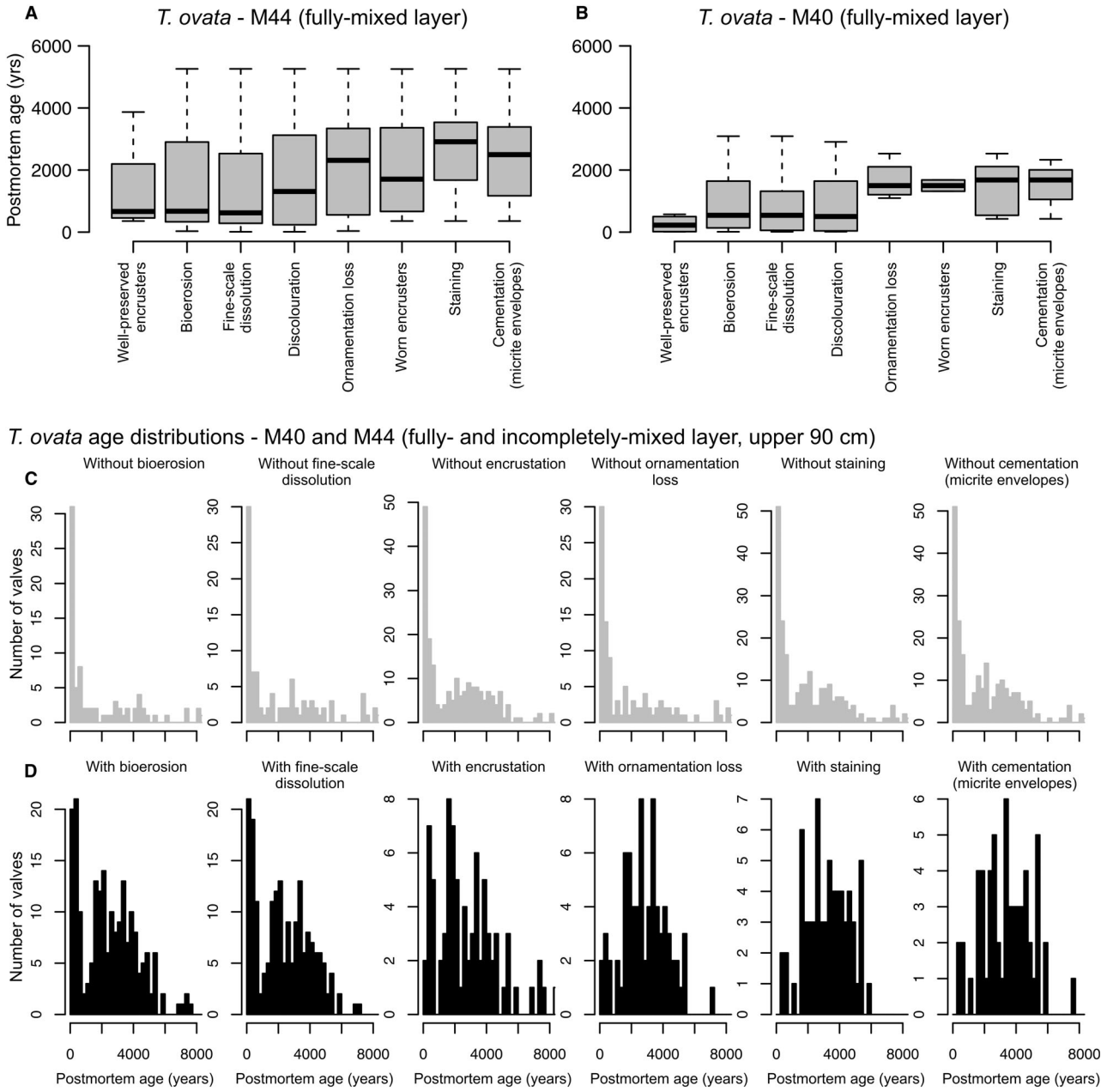

Fig. 9. (A) and (B) Boxplots with postmortem ages of *T. ovata* valves altered by eight variables in the fully-mixed layer (upper *ca* 20 cm). Median ages visualize differences in the timing of skeletal modification among different types of alteration and separate surface alterations (encrustation, bioerosion, fine-scale dissolution, discolouration), subsurface alterations (staining, cementation) and alterations that are a signature of exhumed valves (intense wear of valves leading to loss of ornamentation and worn encrusters), with lower median ages indicating faster alteration. (C) Age distributions of unaltered *T. ovata* valves in the fully-mixed layer and in the underlying layers subjected to incomplete mixing (upper 90 cm) are consistently right-skewed and dominated by valves younger than 500 years (binned to 250 years). (D) Age distributions of *T. ovata* valves in the fully-mixed layer and in the aggradational–highstand unit altered by bioerosion, fine-scale dissolution and encrustation are bimodal, dominated by valves younger than 500 years. Age distributions of valves affected by ornamentation loss, staining and cementation are more symmetrical and dominated by valves older >2000 years; valves younger than 1000 years are rare, indicating that these types of alteration are accrued slowly.

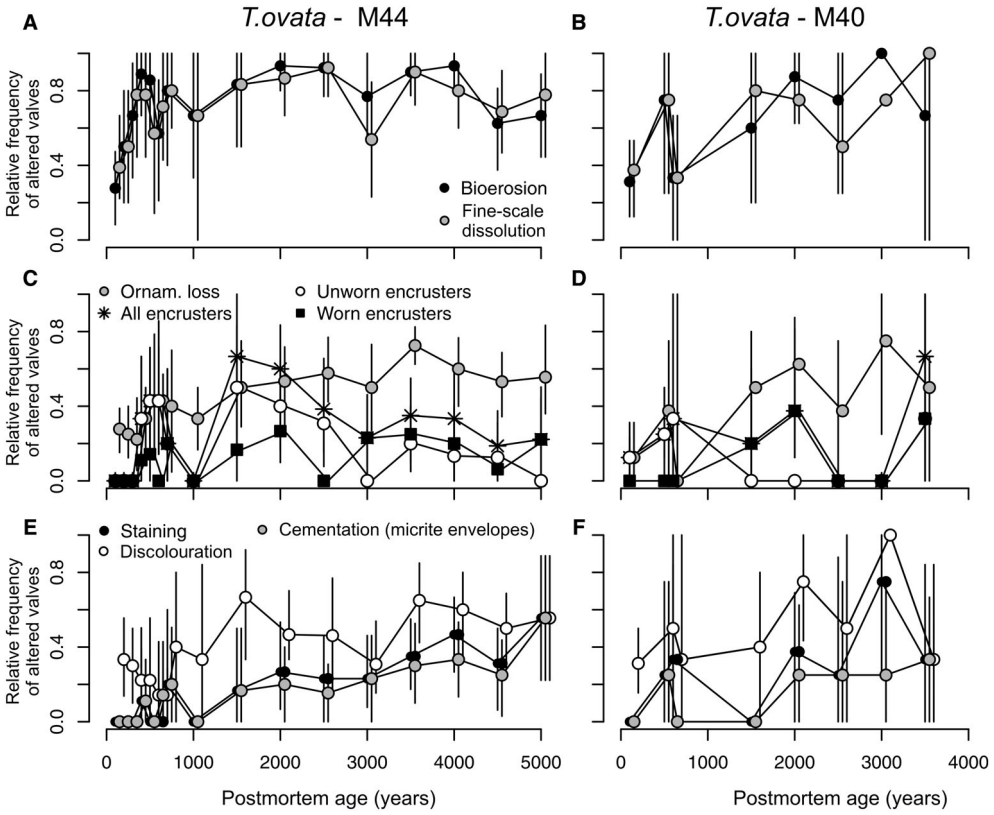

Fig. 10. Cohort-level taphonomic clock that shows the relationships between the frequency of altered valves in age cohorts aggregated to 100 years (valves <1000 years old) and to 500 years (valves >1000 years old) and their post-mortem age in the mixed layer (upper 90 cm). (A) and (B) Frequencies of valves with bioerosion and fine-scale dissolution. (C) and (D) Frequencies of valves with all types of encrusters, well-preserved encrusters, worn encrusters and with worn ornamentation. (E) and (F) Frequencies of stained, cemented and discoloured valves.

cemented valves indicate long residence times in the TAZ and rapid transit below the SZ.

4 Pristine and stained but not encrusted or bored valves indicate rapid burial below the TAZ but long residence times in the SZ. This pathway is rare at Brijuni but can occur if molluscan valves are bored or infested by parasites during their life (and thus exhibit microporosity where cements and nanopyrite can precipitate even with limited residence time in the TAZ). It is noted that precipitation of nanopyritic inclusions alone may probably occur faster in the SZ of fine-grained, iron-and organic-rich sediments.

5 Valves that are encrusted and bored and also stained and cemented indicate long residence times in both the TAZ and SZ.

6 Worn, stained and cemented valves indicate long residence times in both the TAZ and SZ, followed by exhumation to the TAZ.

7 Stained and worn valves with well-preserved encrusters indicate that deep exhumation from the SZ was followed by new colonization by encrusters or borers at the SWI.

The last two pathways correspond to composite alteration that represents a unique signature of deeper subsurface exhumation and develops on durable valves that can cycle through the mixed layer over millennia. The encrustation and bioerosion of shallow-infaunal bivalves (pathway 2) require that they be exhumed from their living position (a few centimetres) to the SWI within the TAZ. This shallow exhumation can be forced by bioturbation or by their emergence to the SWI under oxygen depletion. Nonetheless, the semi-lithified, partly cemented sediments in subsurface zones and the low percentages of clay and silt in the TST and MFZ units suggest that exhumation of stained or cemented valves from

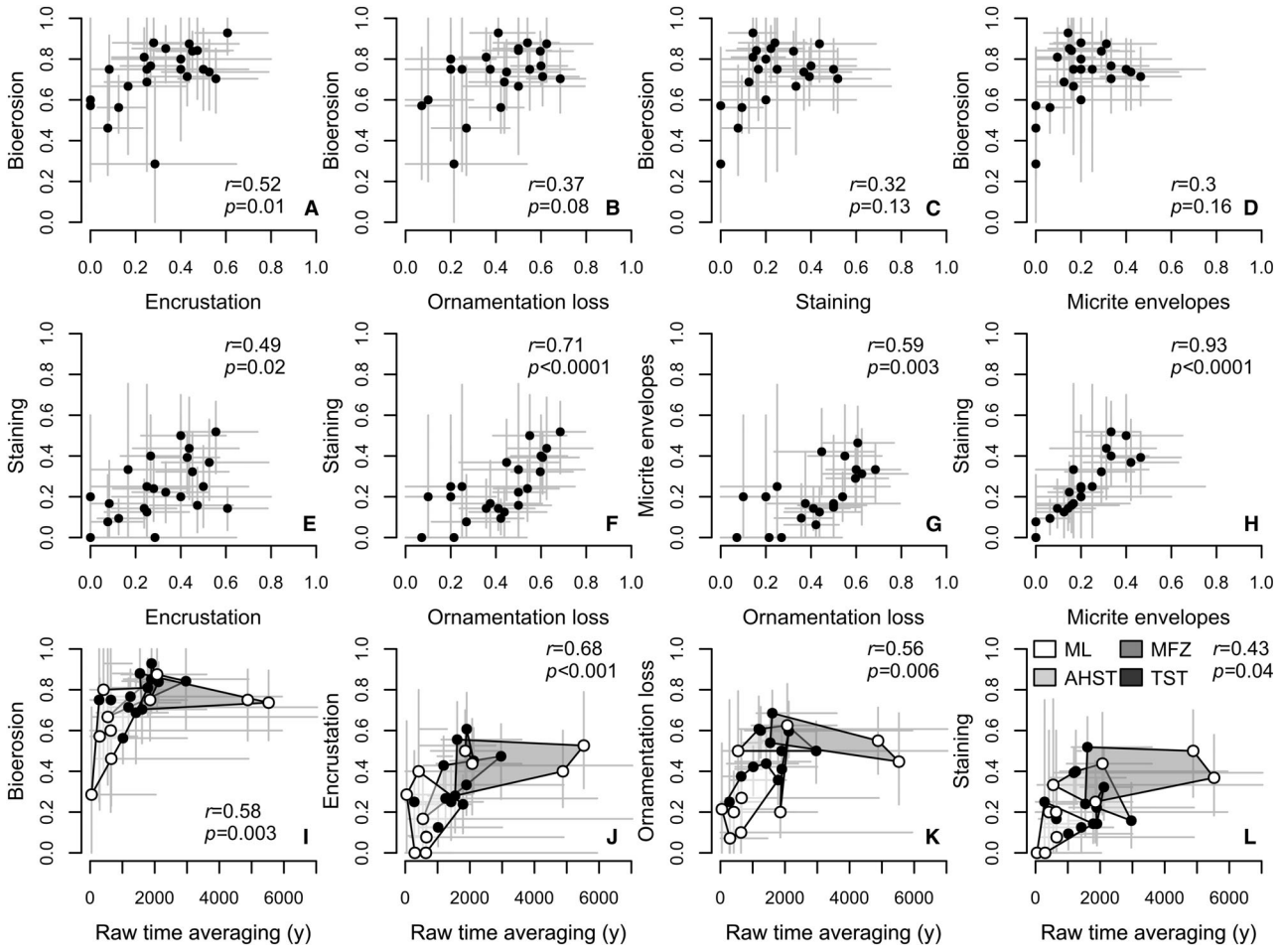

Fig. 11. (A) and (B) Positive correlations between per-increment frequencies of bored and encrusted (A) and bored and worn valves (B). (C) and (D) Although stained and micritized valves are bored, some increments with frequently bored valves do not contain many stained (C) or micritized valves (D) and correlations are thus low. (E) The relationship between per-increment frequencies of staining and encrustation is significantly positive. (F) and (G) Frequencies of staining and micrite envelopes correlate positively with frequencies of worn valves. (H) Frequencies of stained and micritized valves correlate positively. (I) to (L) Positive relationships between raw time averaging (IQR per increment) and per-increment frequencies of valves affected by staining (I), ornamentation loss (J), bioerosion (K) and encrustation (L). Convex hulls correspond to the stratigraphic units. Error bars: 95% bootstrapped confidence intervals.

deeper subsurface levels to the SWI (where they were recolonized by encrusters or borers, leading to composite alteration) was triggered by physical winnowing or erosion. The composite alteration of valves preserved in densely-packed concentrations thus uniquely documents erosion of fine-grained or less durable sediment.

Subsurface increase in the durability of aragonitic valves

High-Mg calcite micrite envelopes, the presence of acicular and dentate cements, and signs of incipient recrystallization indicate that cemented or recrystallized valves were more durable than non-cemented valves when exhumed to the TAZ. The oxidation of pyrite in the TAZ can induce aragonite dissolution of stained valves and thus counteract this effect of authigenic cementation. However, the sequestration model supports the overall increase in durability of valves exhumed from the SZ to the TAZ. Fitting age distributions of *T. ovata* from the fully-mixed layer to the stochastic sequestration model shows that disintegration half-lives of young valves are decadal (*ca* 50 years), i.e. molluscan valves are not expected to last in the

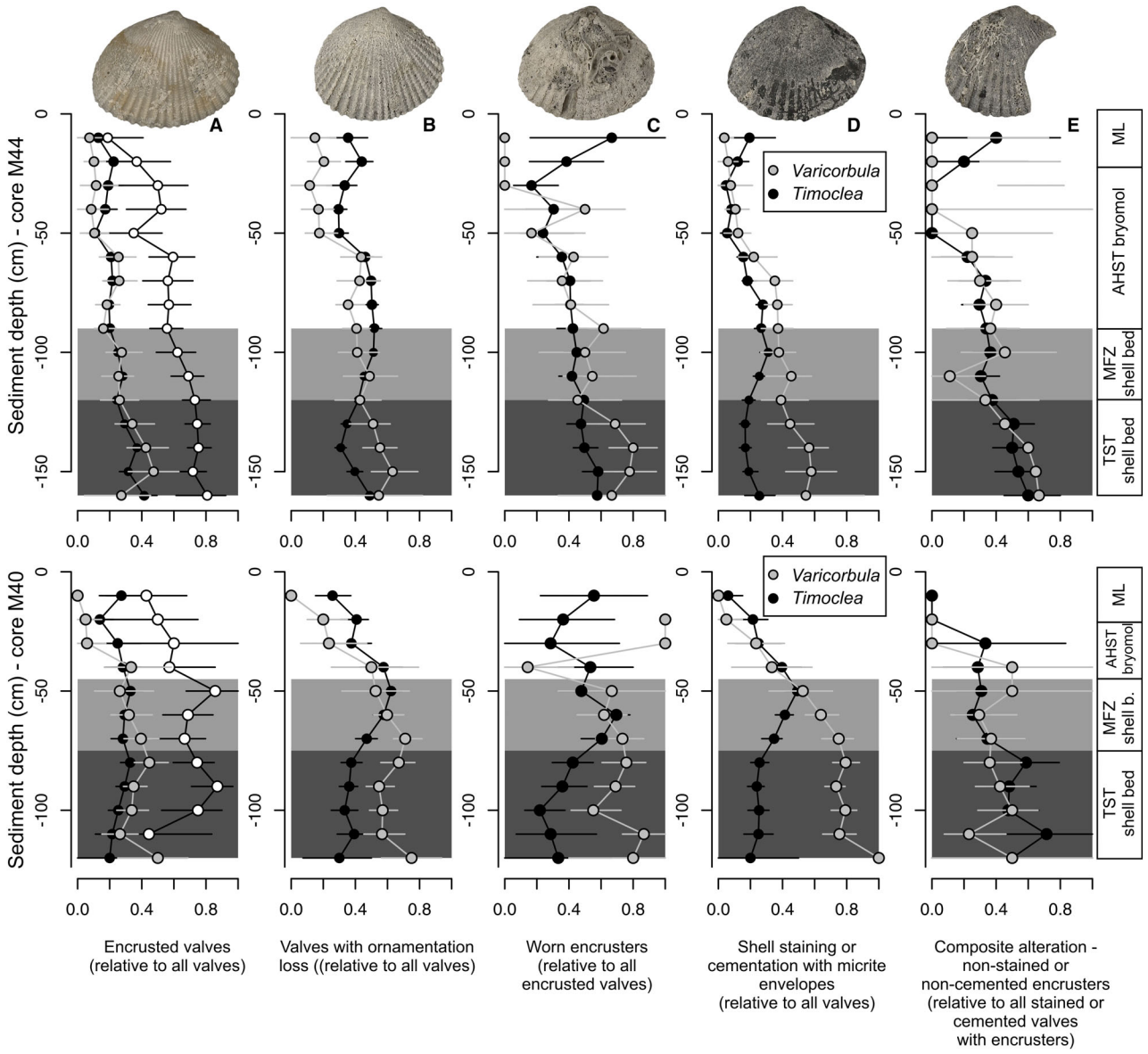

Fig. 12. Stratigraphic decline in the relative frequency of valves with encrusters (A) – white circles correspond to individuals >5 mm – and with worn ornamentation (B), in the frequency of encrusted valves with worn encrusters (C), in the frequency of stained valves (D), and in the frequency of valves with composite alteration (E) in *T. ovata* and *V. gibba* at M44 (top row) and M40 (bottom row). Error bars; 95% bootstrapped confidence intervals. Note: ML – fully mixed layer that consists of a mixture of uppermost AHST and Anthropocene sedimentary particles. For abbreviations please see caption for Fig. 2.

TAZ for several centuries or millennia. However, this sequestration model (AICc = 1502, overperforming a temporally-constant model with AICc = 1556) shows that disintegration is significantly reduced in older valves in the SZ, with half-lives increasing to millennial scales (*ca* 1200 years). This means that old, stained valves and valves with micrite envelopes were more durable when exhumed from the SZ back to the TAZ. Accordingly, the sequestration model with micrite and microspar precipitation in intraskeletal pores and initial neomorphic recrystallization in the anoxic SZ, at depths >20 cm, thus describes the preservation of skeletal particles in lags or at hiatal surfaces averaged to a few millennia. This sequestration mechanism thus explains long persistence of aragonitic valves in the mixed layer by increasing their

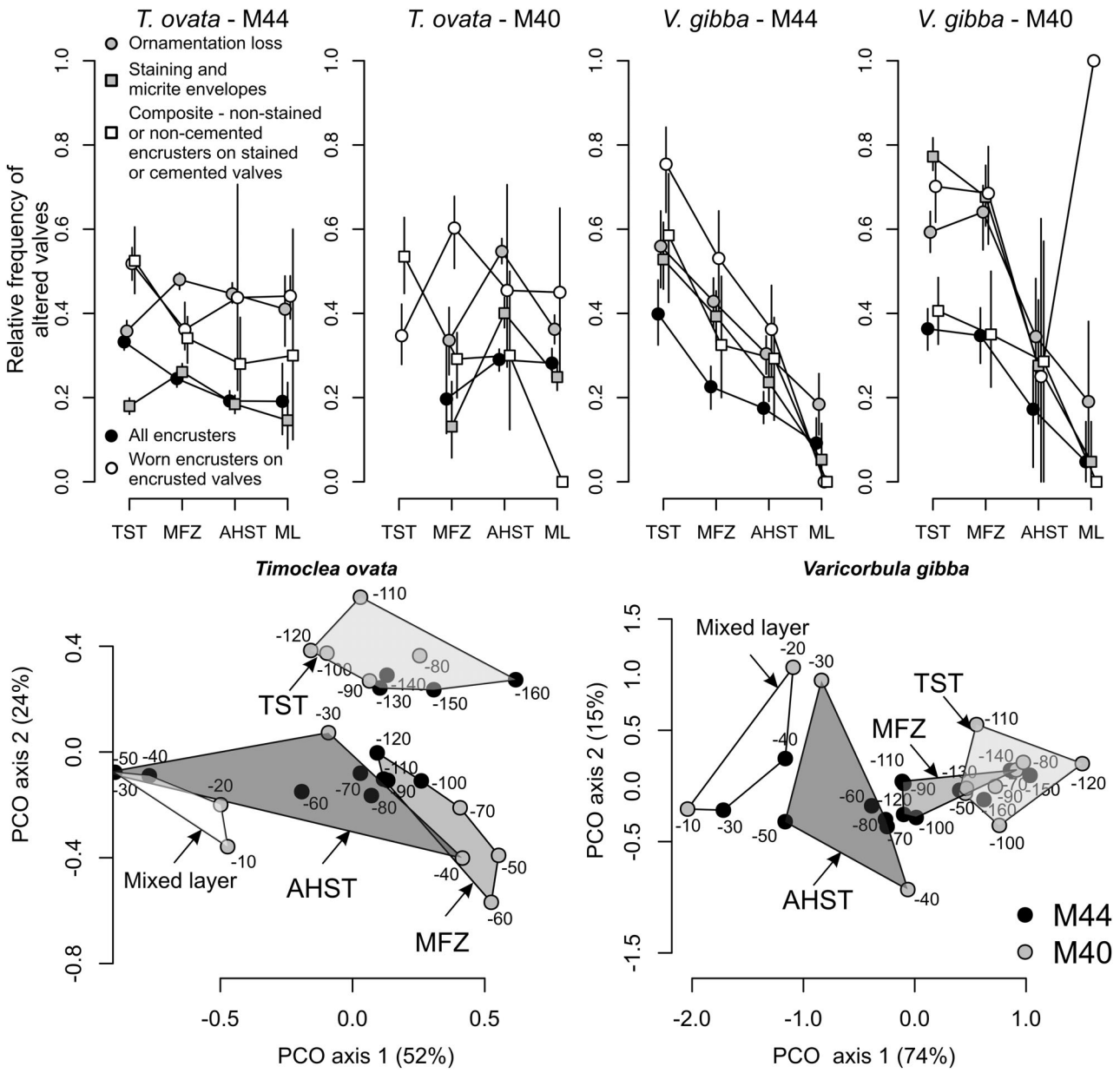

Fig. 13. *Top*: Differences in alteration of *T. ovata* and *V. gibba* between the four stratigraphic units, averaged across values observed in 10 cm thick increments, with 95% bootstrapped confidence intervals. These differences document an upcore decline in the frequency of exhumation–omission–burial cycles in both cores (TST – transgressive increments, MFZ – maximum-flooding zone, AHST – aggradational highstand systems tract, ML – fully-mixed layer). *Bottom*: Increment-level ordination based on all valves shows separation in alteration among the four stratigraphic units. These ordinations are based on five variables (frequencies of encrusted, worn and stained valves, frequencies of valves with ornamentation loss, frequencies of valves with worn encrusters relative to all encrusted valves and frequencies of valves with composite alteration).

durability. The estimates of time averaging based on durable molluscan valves can thus match the millennial-scale time averaging of individual increments inferred from long-term sedimentation rates (mixed depth = 20 cm; Fig. 5). With the exception of the increments in the fully-mixed layer, gravel-sized molluscs at Brijuni thus record the entire duration of increment deposition characterized by a very limited sedimentation rate as in Fig. 1C.

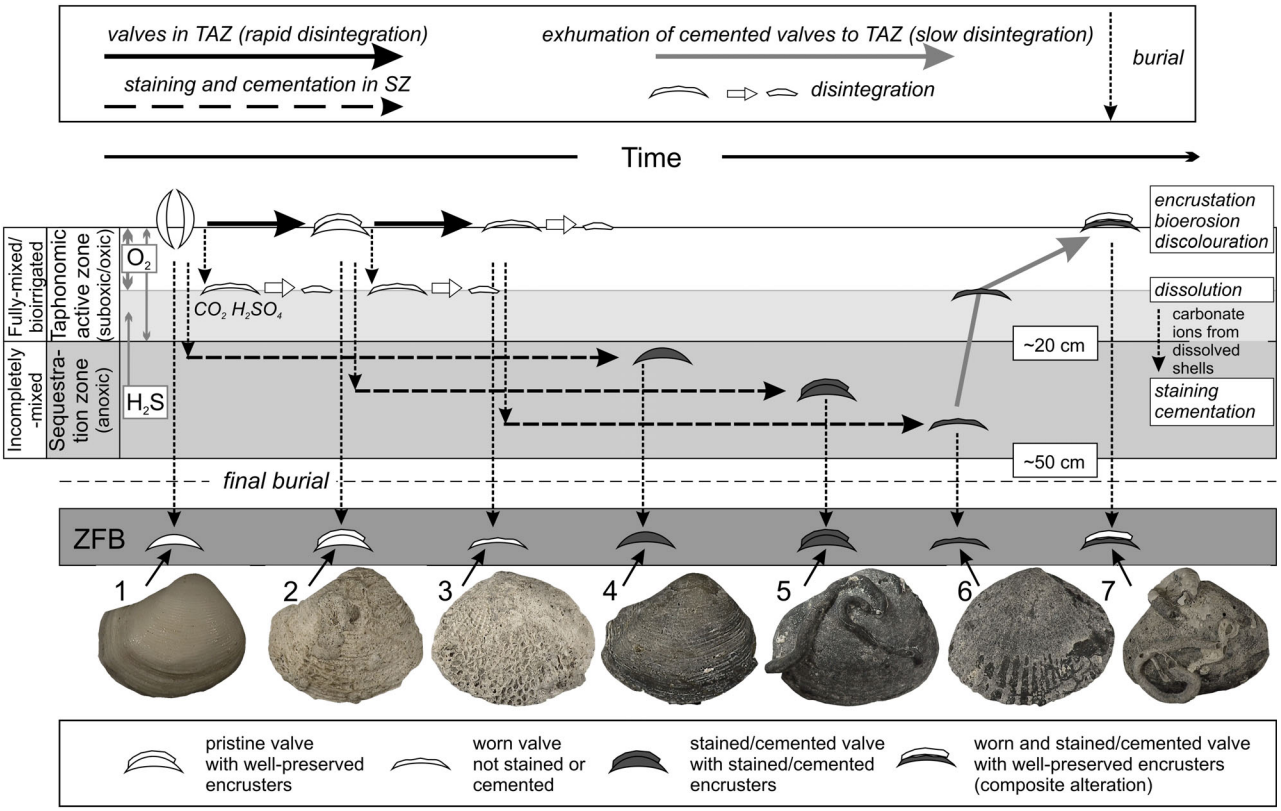

Fig. 14. Preservation pathways of shallow-infaunal bivalves in surface (TAZ) and subsurface (SZ) zones. The boundary between the TAZ and the SZ (*ca* 20 cm at Brijuni) is simplified to a plane but can vary temporally and horizontally due to patchiness in bioturbation and organic matter input. Shells or individual valves can move from the TAZ into the SZ or from the TAZ into the historical layer (zone of final burial, ZFB), or can be exhumed from the SZ to the TAZ independently of each other, for example, by bioturbation. Valves in the historical layer can no longer be exhumed to the SZ. Bioerosion, encrustation (at the SWI) and dissolution (due to exposure to carbonic and sulphuric acids) are rapid in the TAZ (with shorter black solid arrows) and are followed by disintegration if not sequestered. Staining and cementation occur slowly in the subsurface SZ (with longer black dashed arrows), but the valve disintegration rate is reduced due to their transient or permanent burial and cementation (driven by anaerobic degradation of organic matter and by import of carbonate ions from dissolved valves). The disintegration rate of cemented valves is thus also reduced when exhumed to the TAZ. Renewed encrustation of stained and cemented valves is a characteristic signature of deep exhumation (grey arrows). The lengths of horizontal black (solid and dashed) arrows reflect the time needed for alteration in the TAZ and in the SZ. The numbers near valves refer to seven pathways described in the main text.

Taphonomic clock

Analyses confirm that aggregating valves to age cohorts or assemblages reduces the noisiness in the relation between post-mortem age and alteration at the level of individual valves (Powell & Davies, 1990; Meldahl *et al.*, 1997; Kidwell *et al.*, 2005; Tomašových *et al.*, 2006, 2017; Ritter *et al.*, 2017). Such aggregation thus increases the ability of alteration patterns to predict time averaging. For example, burrows intersect and irrigate temporarily anoxic zones in the mixed layer, leading to pH depletion via aerobic decomposition of organic matter and sulphide oxidation (Ku *et al.*, 1999). This process dissolves skeletal particles lining the burrows, whereas skeletal particles in non-irrigated sediments remain protected and well-preserved at the same stratigraphic level. Conversely, a downward movement of sediment by deep-burrowing organisms can rapidly transfer fresh, unaltered skeletal particles below the TAZ and below the SZ. In this scenario, altered, stained and cemented valves that resided in the mixed layer for longer are mixed with pristine valves that were rapidly buried below the mixed layer. Note, however, that this individual-level variability, explaining <10% of variation, is averaged out at

the cohort or assemblage level, where the amount of variation in alteration explained by postmortem age increases to >50%. The assemblage-level alteration thus effectively discriminates between multi-centennial time averaging in the uppermost increments and millennial time averaging. Above all, this discrimination occurs because the high frequency of valves stained by pyrite and cemented by high Mg-calcite micrite uniquely characterizes assemblages averaged to more than 1000 years. Stratigraphic maxima with high frequencies of staining and cementation in the TST and MFZ increments thus point to conditions with unusually long residence times of valves in subsurface zones. Importantly, time averaging does not fully explain variation in assemblage-level alteration because two taphonomic scenarios characterized by a single long-term sedimentation rate but differing in the variability of short-term sedimentation rate can produce assemblages with distinct alteration patterns. First, thin sedimentary increments can form by slow sediment attrition without any erosion close to the SWI. Second, thin sedimentary increments can represent lags that started as thicker, rapidly-deposited increments that were subsequently winnowed (valves that were altered in the SZ were thus exhumed to the SWI). High abundance of valves with composite alteration, as observed in the TST and MFZ units, can be expected to be generated in the second scenario only.

The implications of this difference in variability in short-term sedimentation rate can be explored in a model with random deposition in which the long-term sedimentation rate is constant, the variability in sedimentation (and thus the frequency of burial/exhumation cycles) declines through time (black line in Fig. 15A), and the mixing depth increases from 5 to 30 cm (Fig. 15). For example, under a long-term sedimentation rate of 0.015 cm $year^{-1}$, the residence time within 5 cm increments is expected to be *ca* 333 years. The loss of sediment during the erosional phases compensated by high burial rate naturally translates into higher variability in time averaging in the TST and MFZ increments than in the AHST increments (grey points in Fig. 15B). Therefore, the residence time of valves (and thus time averaging) in 5 cm increments can attain *ca* 1000 years in the TST and MFZ increments (black line in Fig. 15B). This time averaging contrasts with time averaging of 300 to 400 years in the AHST increments. In the absence of mixing by bioturbation, the stratigraphic decline in the short-term variability of the sedimentation rate can be preserved in the stratigraphic record. Mimicking bioturbation by increasing the thickness of increments to 30 cm increases time averaging at all stratigraphic levels. This bioturbation effect, however, averages out the stratigraphic decline in maximum time averaging (grey line in Fig. 15B). If staining or cementation require a residence time of at least 1000 years, then the stained or cemented valves will be preserved in the TST and MFZ units but not in the AHST unit. Similarly, if valves with composite alteration require that they reside in the SZ for at least 1000 years and then are exhumed to the SWI, then such valves will be preserved in the TST and MFZ units. Accordingly, trends in alteration can uniquely detect conditions that temporarily allowed very long residence times of coarse skeletal particles in surface and subsurface zones. The stratigraphic trends in the frequencies of alteration thus detect variability in short-term sedimentation rate even when time averaging and long-term sedimentation rates are constant.

Within-sequence decline in the variability of short-term sedimentation

The upcore decrease in the frequency of encrusted, worn, stained and cemented valves indicates that the residence time of remains in the TAZ (with encrustation) and in the SZ (with staining and micrite envelopes) declined through time. At the same time, the gradual decrease in the frequency of composite alteration associated with the overall decline in grain size also reflects a decline in the frequency of deep exhumation. As the mean sedimentation rate remained constant, the phases with rapid burial (triggered by high production of skeletal carbonate) alternated with deep exhumation during the transgressive phase. In contrast, the depositional dynamic was less volatile during the highstand phase. This decline in variability in short-term sedimentation rate probably reflected an increase in water depth along with reduced wave-induced and current-induced sediment reworking. This deepening, in turn, triggered the transition to epifaunal molluscan and bryozoan communities that trapped fine-grained sediments. Under these conditions, the effective residence times of skeletal particles in the TST and MFZ units can be longer than expected under the long-term sedimentation rate. Such longer residence times are reproduced in the model with random-walk deposition.

The TST increments were thus deposited under conditions characterized by episodic, probably

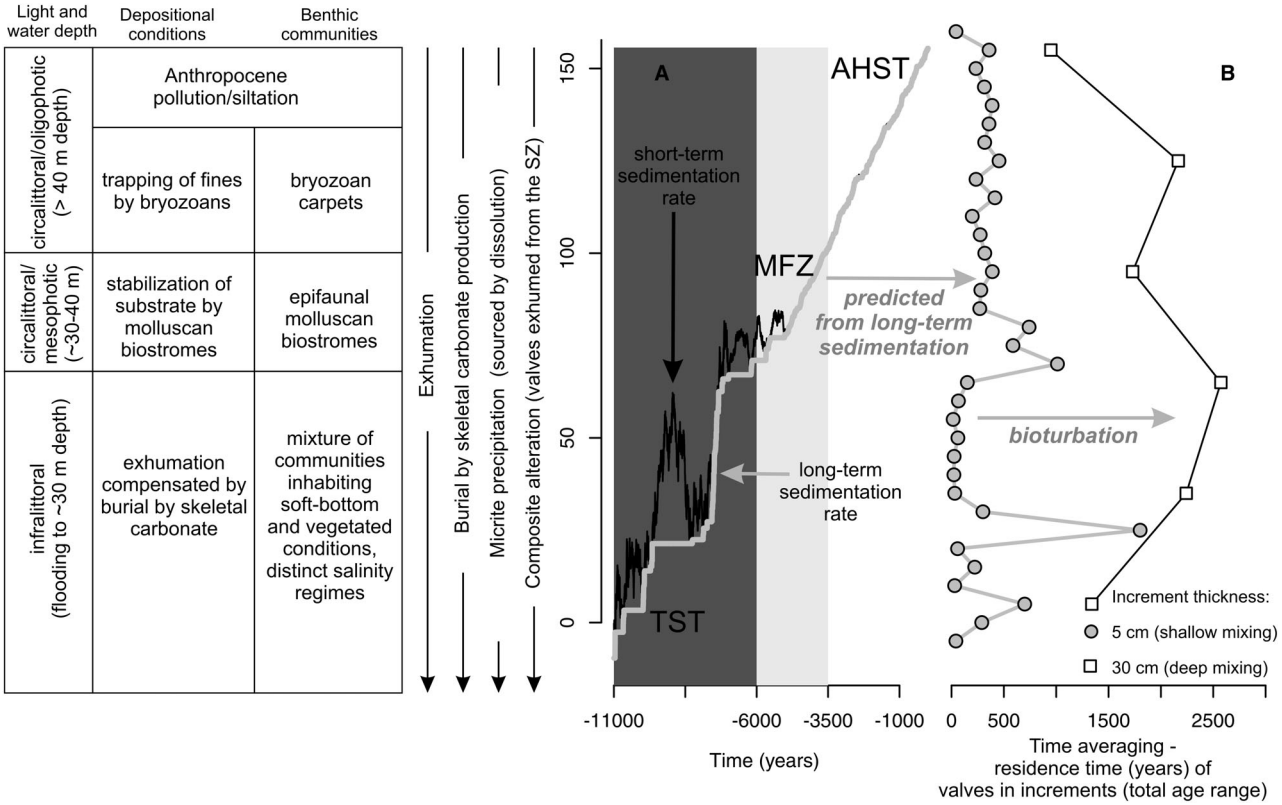

Fig. 15. Depositional changes at Brijuni that are coupled with deepening and with decreasing variability in short-term sedimentation rate – black line in (A), keeping long-term sedimentation rate constant and assuming that disintegration of sediment particles is negligible. This condition is possible when higher sediment erosion or starvation is compensated by higher carbonate production. This leads to a higher effective residence time and higher alteration of durable skeletal particles in the TST and MFZ than in the HST unit. The decoupling between short-term and long-term sedimentation rate is reproduced by a random-walk model in which the net sedimentation rate is constant (0.015 cm $year^{-1}$, grey line in A) over the duration of the model (11 000 years, simulated at yearly steps) but variability in sedimentation rate declines upward (black line in A). This variability is modelled with standard deviations that decline upcore [standard deviation of yearly deposits (TST) = 0.75 cm $year^{-1}$, sd (MFZ) = 0.1 cm $year^{-1}$, sd(AHST) = 0.005 cm $year^{-1}$; see Appendix S2]. The transition from the original chronological variability in short-term sedimentation rate – black line in (A) – to long-term sedimentation rate – grey line in (A) – and to the stratigraphic variability in residence time in the 5 cm thick mixed layer – grey circles in (B) – is modified by sediment erosion. The variability in short-term sedimentation is preserved to some degree if the succession is not mixed by burrowers, as shown by the stratigraphic variability in time averaging of skeletal particles in the 5 cm thick increments – grey circles in (B). If mixing by bioturbation occurs over 30 cm, time averaging – white squares in (B) – increases at all levels but becomes more uniform upcore – horizontal grey arrow in (B).

storm-induced winnowing that alternated with rapid deposition of skeletal carbonate. These conditions ultimately led to accumulation of durable and erosion-resistant skeletal particles (Fig. 15). The mixture of infaunal and epifaunal molluscs (associated with vegetation) in the TST unit indicates that substrate consistency varied through time. The epifauna-dominated communities that form the MFZ shell bed in all cores probably formed spatially widespread, autochthonous or parautochthonous, densely packed biostromes. These biostromes helped to stabilize the SWI, as documented also by the increasing contribution of fines in the uppermost parts of the shell bed. Although seafloor cements triggered by seawater pumping can also be characteristic of the TST–MFZ transition (Caron *et al.*, 2005), it is hypothesized that the micrite cements in these two (TST and MFZ) units initially formed in reducing, low-energy marine conditions in deeper parts of the mixed layer. Accordingly, during the deposition of these units, micrite precipitation

probably led to the formation of incipient firmgrounds when loose surface sediments were winnowed, and cemented valves were exposed to bioerosion and encrustation. Assuming that the upper depth of the SZ is at 20 cm, micrite envelopes on valves located in the TST unit were partly formed during deposition of the MFZ shell bed. Micrite envelopes now located in the MFZ shell bed probably also formed in subsurface zones during the initial deposition of the overlying bryozoan sediments during the highstand phase. The stratigraphic replacement of molluscan communities in the MFZ unit by meadows of erect bryozoans (*Cellaria, Pentapora*) in the AHST unit coincides with declining frequencies of composite alteration. This ecological replacement was associated with temporally less variable sedimentation during the highstand phase and with the establishment of communities with erect bryozoans, which are prolific carbonate producers that can trap fine-grained sediments (Cocito & Ferdeghini, 2001; McKinney & Jaklin, 2001). This shift from molluscan to bryozoan communities mirrors replacements of euphotic, inner or midramp communities by oligophotic, outer-ramp bryozoan communities observed in deepening-upward sequences of the Mediterranean Sea (Pedley & Grasso, 2002; Bassi *et al.*, 2006; Basso *et al.*, 2006; Brandano *et al.*, 2017).

The lack of within-sequence variability in long-term sedimentation

Although the assemblage-level alteration declines across the depositional sequence, it was observed that the long-term sedimentation rate (0.01 to 0.02 cm year^{-1}) and time averaging (*ca* 1000 to 3000 years) did not systematically change through time at Brijuni. It is postulated that long-term sediment accumulation and time averaging of aragonitic bivalves remained constant in spite of changes in accommodation space. The minor variability in the long-term sedimentation rate is probably determined by two factors that minimized and averaged out the temporal variability in short-term sedimentation rate.

1 The production and preservation of skeletal carbonate by molluscs compensated for erosion and winnowing of fine-grained sediments during deposition of the TST and MFZ units, keeping long-term sedimentation rates constant. On the one hand, the positive correlations between the proportion of shell gravel and both ornamentation loss (Spearman $r = 0.58$, $P = 0.027$) and staining (Spearman $r = 0.68$, $P = 0.0065$) indicate that the formation of the TST shelly lag and the MFZ molluscan shell bed at Brijuni was allowed by selective erosion and winnowing of fine-grained sediments. On the other hand, however, several lines of evidence indicate that carbonate production by molluscs also peaked at this time. First, the biostrome-forming oysters and scallops attain the largest sizes in the MFZ shell bed. Second, ecological surveys showed that molluscan biostromes with dense clumps of oysters, *Arca*, scallops, limids and mussels contributed to carbonate accumulation in circalittoral habitats at 20 to 30 m depths during the early and mid-20th century in the north-eastern Adriatic Sea (prior to overfishing and eutrophication; Gamulin-Brida *et al.*, 1968; Gallmetzer *et al.*, 2019; Tomašových *et al.*, 2019b). The MFZ shell bed thus probably represents a similar ecosystem with high population densities of epifaunal bivalves. Third, the proportion of skeletal gravel correlates positively with the frequency of encrusters, indicating that postmortem encrustation was favoured by taphonomic feedback (Spearman $r = 0.77$, $P = 0.0013$). Therefore, the increased accumulation of skeletal dead parts facilitated the colonization of seafloor by carbonate encrusters (Kidwell, 1991b). It is noted that the total thickness of siliciclastic marine sediments deposited during the late transgressive and highstand phases at locations eastward of the prograding Po Delta wedge (at 20 to 30 m) tapers to less than 50 cm and deposits belonging to the HST are effectively missing in central parts of the Gulf of Venice (Correggiari *et al.*, 2001; Cattaneo *et al.*, 2007). These locations were affected by along-shore sediment transport and reworking by currents and storms (Trincardi *et al.*, 1994; Correggiari *et al.*, 1996; Storms *et al.*, 2008; Moscon *et al.*, 2015). The limited thickness at these locations contrasts with the 100 to 160 cm at Brijuni (as observed here) or at Piran (Tomašových *et al.*, 2019). The molluscan and bryozoan communities off Istria, in turn, probably stabilized the seafloor against winnowing. The TST, MFZ and AHST deposits at Brijuni are thus thicker than other age-equivalent and depth-equivalent deposits at non-deltaic locations in the northern Adriatic Sea. The higher thickness thus probably reflects the significant contribution of molluscs and bryozoans to sediment accumulation.

2 The stratigraphic variability in long-term sedimentation rates and in subsurface time averaging is muted by bioturbation. High abundance of *T. ovata* in the transgressive lag – that are younger

than *in situ* oysters and scallops in the shell bed – documents that the shelly record in the TST also contains *T. ovata* individuals that lived during the highstand phase. The stratigraphic divergence in alteration between *V. gibba* and *T. ovata* in the TST increments also indicates that a subset of *T. ovata* valves that lived during the highstand phase were buried into the subsurface TST units (and were exposed for a short time in the TAZ relative to other *T. ovata* valves that were not buried by burrowers).

Implications for the ancient rock record

The cohort-level and assemblage-level taphonomic clocks show that high frequencies of stained valves, valves with micrite envelopes and valves with composite alteration represent indices of high time averaging that exceeds 1000 years. These three preservation states are promising candidates to estimate the minimum timescale of assemblage formation because these processes (staining and micrite precipitation): (i) require a long time to alter skeletal particles; and (ii) increase durability and thus extend survival time of skeletal particles in the mixed layer over the duration of sediment omission. If alteration is fast (for example, as in processes that lead to bioerosion or encrustation), then frequencies of altered valves will not discriminate between assemblages with low and high time averaging. The precipitation of acicular and fibrous cements can be fast in beach rock or in shelf and slope environments, especially under vigorous seawater pumping (Grammer *et al.*, 1999; Van der Kooij *et al.*, 2010). Nonetheless, the precipitation of cryptocrystalline micrite cement in reducing conditions requires that pore waters be exposed to the reaction products for multiple centuries or millennia (to carbonate ions diffusing or advecting from surface zones or from sulphate reduction associated with pyrite precipitation that can increase alkalinity; Raiswell, 1988; Wetzel & Allia, 2000; Mutti & Bernoulli, 2003; Raiswell & Fisher, 2004). The preservation of stained and cemented valves (and such valves that were subsequently encrusted or bored at the SWI) thus indicates very low sedimentation rates in marine environments. Furthermore, cementation by high-Mg calcitic micrite increases valve durability and thus promotes the accumulation of valves in the mixed layer at millennial scales even if they are exhumed from the SZ to the TAZ. In the absence of cementation or other diagenetic stabilization, valves in the TAZ would disintegrate quickly (at decadal scales). This timescale of disintegration means they would not track the duration of longer, millennial-scale hiatuses associated with skeletal lags or concentrations. The criteria for detecting millennial-scale time averaging based on valves with cements and with composite alteration can be applied to Palaeozoic, Mesozoic and Cenozoic deposits in environments prone to subsurface cementation in the mixed layer (Zamora *et al.*, 2008; Vodrážka *et al.*, 2009; Fernández-López, 2011; Wilson *et al.*, 2012; Coimbra & Duarte, 2020). For example, repeated exhumation of skeletal particles initially cemented in subsurface conditions is suggested by the encrustation and bioerosion of exhumed concretions (Kennedy & Garrison, 1975; Fürsich, 1978; Fürsich *et al.*, 1992; Hesselbo & Palmer, 1992). This burial/exhumation scenario is also supported by the encrustation and bioerosion of moulds that were dissolved in semi-lithified sediment (Palmer & Wilson, 2004; Tomašových & Schlögl, 2008).

CONCLUSIONS

Measurements of assemblage-level alteration can identify millennial-scale hiatuses or condensed intervals, and thus can be used to estimate stratigraphic variability in temporal resolution within depositional sequences in the ancient rock record. First, residence times exceeding 1000 years in the mixed layer are needed to stain and cement >50% of valves, indicating that rates of pervasive staining and micrite cementation are very slow in the reducing subsurface zones of the mixed layer. Second, precipitation of micritic and microsparitic cements in intraskeletal pores enables long-term preservation of valves exhumed from the sequestration zone (SZ) in the taphonomic active zone (TAZ). This cementation, in turn, allows the repeated boring and encrustation of old and durable valves exhumed to the sediment–water interface. The high frequency of valves stained by pyrite, valves with micrite envelopes, and valves with composite alteration thus indicates that fossil assemblages with these attributes are time-averaged to millennial scales.

Although alteration of durable skeletal particles tracks to some degree long-term sedimentation rate and time averaging, it also gives insights into short-term dynamics in sedimentation that is later lost via erosion of finer sediments or averaged out by bioturbation because valves buried in

subsurface and later exhumed bear a unique signature of subsurface staining or cementation overprinted by borers or encrusters. The upcore decline in the frequency of valves with composite alteration thus indicates high frequency of sediment winnowing during the transgressive phase and a slow but persistent positive sedimentation during the highstand phase. As long-term sedimentation rates and time averaging remained rather constant within the depositional sequence, the production and stabilization of carbonate sediments by molluscs compensated for the winnowing of sediment fines.

ACKNOWLEDGEMENTS

We thank Christian Betzler, Vincent Caron and three anonymous reviewers for critical reviews, and members of the Stratigraphic Paleoecology class at the University of Vienna for discussions. We thank the captain of the coring vessel *Manta Bianca*, Jernej Sedmak for the campaign in summer 2013 and Sergii Kurylo and Tomáš Mikuš for help with microprobe measurements. This work was funded by the Austrian Science Fund (FWF project P24901), the Slovak Research and Development Agency (APVV 17-0155), the Slovak Scientific Grant Agency (VEGA 0169/19) and the Ida Pfeiffer Professorship 2020 to A.T. at the University of Vienna. Shell dating was supported by a grant of the University of Vienna (Austria) to Martin Zuschin.

DATA AVAILABILITY STATEMENT

Geochronological and taphonomic data are available in the Tables S1 and S2 and scripts are available in Appendix S1 and S2.

REFERENCES

Alexandersson, E.T. (1972a) Micritization of carbonate particles: processes of precipitation and dissolution in modern shallow-marine sediments. *Univ. Uppsala Geol. Inst. Bull.*, **7**, 201–236.

Alexandersson, E.T. (1972b) Intragranular growth of marine aragonite and Mg-calcite; evidence of precipitation from supersaturated seawater. *J. Sed. Res.*, **42**, 441–460.

Allen, A.P., **Kosnik, M.A.** and **Kaufman, D.S.** (2013) Characterizing the dynamics of amino acid racemization using time-dependent reaction kinetics: a Bayesian approach to fitting age-calibration models. *Quat. Geochronol.*, **18**, 63–77.

Aller, R.C. (1994) Bioturbation and remineralization of sedimentary organic matter: effects of redox oscillation. *Chem. Geol.*, **114**, 331–345.

Allouc, J. (1990) Quaternary crusts on slopes of the Mediterranean Sea: a tentative explanation for their genesis. *Mar. Geol.*, **94**, 205–238.

Amorosi, A. (1995) Glaucony and sequence stratigraphy; a conceptual framework of distribution in siliciclastic sequences. *J. Sed. Res.*, **65**, 419–425.

Amorosi, A., **Bruno, L.**, **Campo, B.**, **Morelli, A.**, **Rossi, V.**, **Scarponi, D.**, **Hong, W.**, **Bohacs, K.M.** and **Drexler, T.M.** (2017) Global sea-level control on local parasequence architecture from the Holocene record of the Po Plain, Italy. *Mar. Petrol. Geol.*, **87**, 99–111.

Amorosi, A., **Fontana, A.**, **Antonioli, F.**, **Primon, S.** and **Bondesan, A.** (2008) Post-LGM sedimentation and Holocene shoreline evolution in the NW Adriatic coastal area. *GeoActa*, **7**, 41–67.

Amorosi, A. and **Sammartino, I.** (2018) Shifts in sediment provenance across a hierarchy of bounding surfaces: a sequence-stratigraphic perspective from bulk-sediment geochemistry. *Sed. Geol.*, **375**, 145–156.

Anderson, M.J. and **Walsh, D.C.** (2013) PERMANOVA, ANOSIM, and the Mantel test in the face of heterogeneous dispersions: what null hypothesis are you testing? *Ecol. Monogr.*, **83**, 557–574.

Andrieu, S., **Brigaud, B.**, **Barbarand, J.** and **Lasseur, E.** (2018) The complex diagenetic history of discontinuities in shallow-marine carbonate rocks: new insights from high-resolution ion microprobe investigation of δ18O and δ13C of early cements. *Sedimentology*, **65**, 360–399.

Antonioli, F., **Anzidei, M.**, **Lambeck, K.**, **Auriemma, R.**, **Gaddi, D.**, **Furlani, S.**, **Orrù, P.**, **Solinas, E.**, **Gaspari, A.**, **Karinja, S.**, **Kovačić, V.** and **Surace, L.** (2007) Sea-level change during the Holocene in Sardinia and in the northeastern Adriatic (central Mediterranean Sea) from archaeological and geomorphological data. *Quatern. Sci. Rev.*, **26**, 2463–2486.

Asioli, A., **Trincardi, F.**, **Lowe, J.J.**, **Ariztegui, D.**, **Langone, L.** and **Oldfield, F.** (2001) Sub-millennial scale climatic oscillations in the central Adriatic during the Late glacial: palaeoceanographic implications. *Quatern. Sci. Rev.*, **20**, 1201–1221.

Bassi, D., **Carannante, G.**, **Murru, M.**, **Simone, L.** and **Toscano, F.** (2006) Rhodalgal/bryomol assemblages in temperate-type carbonate, channelized depositional systems: the Early Miocene of the Sarcidano area (Sardinia, Italy). *Geol. Soc. London Spec. Publ.*, **255**, 35–52.

Basso, D., **Morbioli, C.** and **Corselli, C.** (2006) Rhodolith facies evolution and burial as a response to Holocene transgression at the Pontian Islands shelf break. *Geol. Soc. London Spec. Public.*, **255**, 23–34.

Bathurst, R.G.C. (1966) Boring algae, micrite envelopes and lithification of molluscan biosparites. *Geol. J.*, **5**, 15–32.

Baumgartner, L.K., **Reid, R.P.**, **Dupraz, C.**, **Decho, A.W.**, **Buckley, D.H.**, **Spear, J.R.**, **Przekop, K.M.** and **Visscher, P.T.** (2006) Sulfate reducing bacteria in microbial mats: changing paradigms, new discoveries. *Sed. Geol.*, **185**, 131–145.

Best, M.M., **Ku, T.C.**, **Kidwell, S.M.** and **Walter, L.M.** (2007) Carbonate preservation in shallow marine environments: unexpected role of tropical siliciclastics. *J. Geol.*, **115**, 437–456.

Brady, M. (2018) Testing patterns of association between brachiopod bioclast deposits and stratigraphic discontinuities: a case study in middle–upper Devonian carbonate-dominated settings of North America. *J. Geol.*, **126**, 141–164.

Brady, M. and **Bowie, C.** (2017) Discontinuity surfaces and microfacies in a storm-dominated shallow epeiric sea, Devonian Cedar Valley Group, Iowa. *Depositional Rec.*, **3**, 136–160.

Braga, J.C., **Puga-Bernabéu, Á.**, **Heindel, K.**, **Patterson, M.A.**, **Birgel, D.**, **Peckmann, J.**, **Sanchez-Almazo, I.M.**, **Webster, J.M.**, **Yokogama, Y.** and **Riding, R.** (2019) Microbialites in Last glacial maximum and deglacial reefs of the Great Barrier Reef (IODP Expedition 325, NE Australia). *Palaeogeogr. Palaeoclimatol. Palaeoecol.*, **514**, 1–17.

Brand, U. and **Morrison, J.O.** (1987) Diagenesis and pyritization of crinoid ossicles. *Can. J. Earth Sci.*, **24**, 2486–2498.

Brandano, M. and **Civitelli, G.** (2007) Non-seagrass meadow sedimentary facies of the Pontinian Islands, Tyrrhenian Sea: a modern example of mixed carbonate–siliciclastic sedimentation. *Sed. Geol.*, **201**, 286–301.

Brandano, M., **Cornacchia, I.** and **Tomassetti, L.** (2017) Global versus regional influence on the carbonate factories of Oligo-Miocene carbonate platforms in the Mediterranean area. *Mar. Pet. Geol.*, **87**, 188–202.

Brigaud, B., **Andrieu, S.**, **Blaise, T.**, **Haurine, F.** and **Barbarand, J.** (2021) Calcite uranium–lead geochronology applied to hardground lithification and sequence boundary dating. *Sedimentology*, **68**, 168–195.

Broecker, W.S., **Andree, M.**, **Bonani, G.**, **Wolfli, W.**, **Klas, M.**, **Mix, A.** and **Oeschger, H.** (1988) Comparison between radiocarbon ages obtained on coexisting planktonic foraminifera. *Paleoceanography*, **3**, 647–657.

Bruno, L., **Bohacs, K.M.**, **Campo, B.**, **Drexler, T.M.**, **Rossi, V.**, **Sammartino, I.**, **Scarponi, D.**, **Hong, W.** and **Amorosi, A.** (2017) Early Holocene transgressive palaeogeography in the Po coastal plain (northern Italy). *Sedimentology*, **64**, 1792–1816.

Brunović, D., **Miko, S.**, **Hasan, O.**, **Papatheodorou, G.**, **Ilijanić, N.**, **Miserocchi, S.**, **Correggiari, A.** and **Geraga, M.** (2020) Late Pleistocene and Holocene paleoenvironmental reconstruction of a drowned karst isolation basin (Lošinj Channel, NE Adriatic Sea). *Palaeogeogr. Palaeoclimatol. Palaeoecol.*, **544**, 109587.

Burns, F.E., **Burley, S.D.**, **Gawthorpe, R.L.** and **Pollard, J.E.** (2005) Diagenetic signatures of stratal surfaces in the Upper Jurassic Fulmar Formation, central North Sea, UKCS. *Sedimentology*, **52**, 1155–1185.

Capozzi, R., **Guido, F.L.**, **Oppo, D.** and **Gabbianelli, G.** (2012) Methane-derived authigenic carbonates (MDAC) in northern-central Adriatic Sea: relationships between reservoir and methane seepages. *Mar. Geol.*, **332**, 174–188.

Caratelli, M., **Archuby, F.M.**, **Fürsich, F.** and **Pignatti, J.** (2021) Macroids from mixed siliciclastic-carbonate high-frequency sequences of the Agrio Formation (Lower Cretaceous), Neuquén Basin: palaeoecological and palaeoenvironmental constraints. *Cretac. Res.*, **123**, 104778.

Caron, V., **Nelson, C.S.** and **Kamp, P.J.** (2005) Sequence stratigraphic context of syndepositional diagenesis in cool-water shelf carbonates: Pliocene limestones, New Zealand. *J. Sed. Res.*, **75**, 231–250.

Caron, V., **Nelson, C.S.**, **Kamp, P.J.**, **Morad, S.**, **Ketzler, J.M.** and **De Ros, L.F.** (2012) Linkages between tapho-diagenesis and sequence stratigraphy in cool-water limestones from a Pliocene forearc seaway, New Zealand. *Linking Diagenesis Sequence Stratigr Int. Assoc. Sedimentol. Spec. Public.*, **45**, 445–476.

Cattaneo, A. and **Trincardi, F.** (1999) The Late Quaternary transgressive record in the Adriatic epicontinental sea: basin widening and facies partitioning. In: *Isolated Shallow Marine Sand Bodies Sequence Stratigraphic Analysis and Sedimentologic Interpretation* (Eds Bergman, K.M. and Snedden, J.W.), *SEPM Special Publication*, **64**, 127–146.

Cattaneo, A., **Trincardi, F.**, **Asioli, A.** and **Correggiari, A.** (2007) The Western Adriatic shelf clinoform: energy-limited bottomset. *Cont. Shelf Res.*, **27**, 506–525.

Catuneanu, O. (2019a) Scale in sequence stratigraphy. *Mar. Petrol. Geol.*, **106**, 128–159.

Catuneanu, O. (2019b) Model-independent sequence stratigraphy. *Earth-Sci. Rev.*, **188**, 312–388.

Cherns, L., **Wheeley, J.R.** and **Wright, V.P.** (2008) Taphonomic windows and molluscan preservation. *Palaeogeogr. Palaeoclimatol. Palaeoecol.*, **270**, 220–229.

Christ, N., **Immenhauser, A.**, **Wood, R.A.**, **Darwich, K.** and **Niedermayr, A.** (2015) Petrography and environmental controls on the formation of Phanerozoic marine carbonate hardgrounds. *Earth Sci. Rev.*, **151**, 176–226.

Clari, P.A. and **Martire, L.** (1996) Interplay of cementation, mechanical compaction, and chemical compaction in nodular limestones of the Rosso Ammonitico Veronese (Middle-Upper Jurassic, northeastern Italy). *J. Sediment. Res.*, **66**, 447–458.

Clari, P.A., **Pierre, F.D.** and **Martire, L.** (1995) Discontinuities in carbonate successions: identification, interpretation and classification of some Italian examples. *Sed. Geol.*, **100**, 97–121.

Cocito, S. and **Ferdeghini, F.** (2001) Carbonate standing stock and carbonate production of the bryozoan *Pentapora fascialis* in the North-Western Mediterranean. *Facies*, **45**, 25–30.

Coimbra, R. and **Duarte, L.V.** (2020) The distinctive character of lumpy limestones (Early Jurassic, Lusitanian Basin, W Portugal). *Geol. J.*, **55**, 1003–1022.

Correggiari, A., **Field, M.E.** and **Trincardi, F.** (1996) Late Quaternary transgressive large dunes on the sediment-starved Adriatic shelf. *Geol. Soc. London Spec. Public.*, **117**, 155–169.

Correggiari, A., **Trincardi, F.**, **Langone, L.** and **Roveri, M.** (2001) Styles of failure in late Holocene highstand prodelta wedges on the Adriatic shelf. *J. Sediment. Res.*, **71**, 218–236.

Corselli, C., **Basso, D.** and **Garzanti, E.** (1994) Paleobiological and sedimentological evidence of Pleistocene/Holocene hiatuses and ironstone formation at the Pontian Islands shelfbreak (Italy). *Mar. Geol.*, **117**, 317–328.

Davies, D.J., **Powell, E.N.** and **Stanton Jr., R.J.** (1989) Relative rates of shell dissolution and net sediment accumulation-a commentary: can shell beds form by the gradual accumulation of biogenic debris on the sea floor? *Lethaia*, **22**, 207–212.

Davies, N.S., **Shillito, A.P.** and **McMahon, W.J.** (2019) Where does the time go? Assessing the chronostratigraphic fidelity of sedimentary geological outcrops in the Pliocene-Pleistocene Red Crag Formation, eastern England. *J. Geol. Soc.*, **176**, 1154–1168.

Deville de Periere, M., **Durlet, C.**, **Vennin, E.**, **Lambert, L.**, **Bourillot, R.**, **Caline, B.** and **Poli, E.** (2011) Morphometry of micrite particles in cretaceous microporous limestones of the Middle East: influence on reservoir properties. *Mar. Petrol. Geol.*, **28**, 1727–1750.

Dickson, J.A.D., **Wood, R.A.**, **Al Rougha, H.B.** and **Shebl, H.** (2008) Sulphate reduction associated with hardgrounds: lithification afterburn! *Sed. Geol.*, **205**, 34–39.

Dominguez, J.G., **Kosnik, M.**, **Allen, A.P.**, **Hua, Q.**, **Jacob, D.E.**, **Kaufman, D.S.** and **Whitacre, K.** (2016) Time-averaging and stratigraphic resolution in death assemblages and Holocene deposits: Sydney Harbour's molluscan record. *Palaios*, **31**, 563–574.

Dominici, S. (2001) Taphonomy and paleoecology of shallow marine macrofossil assemblages in a collisional setting (late Pliocene–early Pleistocene, western Emilia, Italy). *Palaios*, **16**, 336–353.

Faivre, S., **Fouache, E.**, **Ghilardi, M.**, **Antonioli, F.**, **Furlani, S.** and **Kovačić, V.** (2011) Relative sea level change in western Istria (Croatia) during the last millennium. *Quatern. Int.*, **232**, 132–143.

Felja, I., **Fontana, A.**, **Furlani, S.**, **Bajraktarević, Z.**, **Paradžik, A.**, **Topalović, E.**, **Rossato, S.**, **Ćosović, V.** and **Juračić, M.** (2015) Environmental changes in the lower Mirna River valley (Istria, Croatia) during Upper Holocene. *Geol. Croatica*, **68**, 209–224.

Fernández-López, S.R. (2011) Taphonomic analysis and sequence stratigraphy of the Albarracinites beds (lower Bajocian, Iberian Range, Spain). An example of shallow condensed section. *Bull. Soc. Géol. Fr.*, **182**, 405–415.

Flessa, K.W., **Cutler, A.H.** and **Meldahl, K.H.** (1993) Time and taphonomy: quantitative estimates of time-averaging and stratigraphic disorder in a shallow marine habitat. *Paleobiology*, **19**, 266–286.

Fürsich, F.T. (1978) The influence of faunal condensation and mixing on the preservation of fossil benthic communities. *Lethaia*, **11**, 243–250.

Fürsich, F.T. (1979) Genesis, environment and ecology of Jurassic hardgrounds. *Neues Jahrbuch für Geologie und Paläontologie, Abhandlungen*, **158**, 1–63.

Fürsich, F.T., **Oschmann, W.**, **Singh, I.B.** and **Jaitly, A.K.** (1992) Hardgrounds, reworked concretion levels and condensed horizons in the Jurassic of western India: their significance for basin analysis. *J. Geol. Soc.*, **149**, 313–331.

Fütterer, D. (1969) Die Sedimente der nördlichen Adria vor der Küste Istriens. *Göttinger Arbeiten zur Geologie und Paläontologie*, **3**, 1–57.

Gallagher, K.L., **Kading, T.J.**, **Braissant, O.**, **Dupraz, C.** and **Visscher, P.T.** (2012) Inside the alkalinity engine: the role of electron donors in the organomineralization potential of sulfate-reducing bacteria. *Geobiology*, **10**, 518–530.

Gallmetzer, I., **Haselmair, A.**, **Stachowitsch, M.** and **Zuschin, M.** (2016) An innovative piston corer for large-volume sediment samples. *Limnol. Oceanogr. Methods*, **14**, 698–717.

Gallmetzer, I., **Haselmair, A.**, **Tomašových, A.**, **Mautner, A.K.**, **Schnedl, S.M.**, **Cassin, D.**, **Zonta, R.** and **Zuschin, M.** (2019) Tracing origin and collapse of Holocene benthic baseline communities in the northern Adriatic Sea. *Palaios*, **34**, 121–145.

Gamulin-Brida, H., **Pozar, A.** and **Zavodnik, D.** (1968) Contributions aux recherches sur la bionomie benthique des fonds meubles de l'Adriatique du nord (II). *Bioloski Glasnik*, **21**, 157–201.

García-Ramos, D.A. and **Zuschin, M.** (2019) High-frequency cycles of brachiopod shell beds on subaqueous delta-scale clinoforms (early Pliocene, south-east Spain). *Sedimentology*, **66**, 1486–1530.

Ge, Y., **Lokier, S.W.**, **Hoffmann, R.**, **Pederson, C.L.**, **Neuser, R.D.** and **Immenhauser, A.** (2020a) Composite micrite envelopes in the lagoon of Abu Dhabi and their application for the recognition of ancient firm-to hardgrounds. *Mar. Geol.*, **423**, 106141.

Ge, Y., **Pederson, C.L.**, **Lokier, S.W.**, **Traas, J.P.**, **Nehrke, G.**, **Neuser, R.D.**, **Goetschl, K.E.** and **Immenhauser, A.** (2020b) Late Holocene to Recent aragonite-cemented transgressive lag deposits in the Abu Dhabi lagoon and intertidal sabkha. *Sedimentology*, **67**, 2426–2454.

Godet, A. (2013) Drowning unconformities: palaeoenvironmental significance and involvement of global processes. *Sed. Geol.*, **293**, 45–66.

Gómez Fernández, J.J. and **Fernández López, S.R.** (1994) Condensation processes in shallow platforms. *Sed. Geol.*, **92**, 147–159.

Grammer, G.M., **Crescini, C.M.**, **McNeill, D.F.** and **Taylor, L.H.** (1999) Quantifying rates of syndepositional marine cementation in deeper platform environments-new insight into a fundamental process. *J. Sediment. Res.*, **69**, 202–207.

Green, M.A., **Aller, R.C.** and **Aller, J.Y.** (1993) Carbonate dissolution and temporal abundances of foraminifera in Long Island Sound sediments. *Limnol. Oceanogr.*, **38**, 331–345.

Hendry, J.P., **Wilkinson, M.**, **Fallick, A.E.** and **Trewin, N.H.** (2000) Disseminated 'jigsaw piece'dolomite in Upper Jurassic shelf sandstones, Central North Sea: an example of cement growth during bioturbation? *Sedimentology*, **47**, 631–644.

Hendy, A.J., **Kamp, P.J.** and **Vonk, A.J.** (2006) Cool-water shell bed taphofacies from Miocene-Pliocene shelf sequences in New Zealand: utility of taphofacies in sequence stratigraphic analysis. *Geol. Soc. London Spec. Public.*, **255**, 283–305.

Hesselbo, S.P. and **Palmer, T.J.** (1992) Reworked early diagenetic concretions and the bioerosional origin of a regional discontinuity within British Jurassic marine mudstones. *Sedimentology*, **39**, 1045–1065.

Hillgärtner, H. (1998) Discontinuity surfaces on a shallow-marine carbonate platform (Berriasian, Valanginian, France and Switzerland). *J. Sediment. Res.*, **68**, 1093–1108.

Holbrook, J. and **Miall, A.D.** (2020) Time in the rock: a field guide to interpreting past events and processes from a fragmentary siliciclastic archive. *Earth Sci. Rev.*, **203**, 103121.

Holland, S.M. (2000) The quality of the fossil record: a sequence stratigraphic perspective. *Paleobiology*, **26** (Supplement), 148–168.

Holmes, S.P. and **Miller, N.** (2006) Aspects of the ecology and population genetics of the bivalve *Varicorbula gibba*. *Mar. Ecol. Prog. Ser.*, **315**, 129–140.

Hu, X. and **Burdige, D.J.** (2008) Shallow marine carbonate dissolution and early diagenesis—implications from an incubation study. *J. Mar. Res.*, **66**, 489–527.

Jakl, Z. (2012) Kartiranje morskih staništa i vrsta Nacionalnog parka Brijuni (2010–2011). Izvještaj, Udruga Sunce, Split, 1–8.

Jarochowska, E., **Nohl, T.**, **Grohganz, M.**, **Hohmann, N.**, **Vandenbroucke, T.R.A.** and **Munnecke, A.** (2020) Reconstructing depositional rates and their effect on paleoenvironmental proxies: the case of the Lau Carbon Isotope Excursion in Gotland, Sweden. *Paleoceanogr. Paleoclimatol.*, **35**, e2020PA003979.

Jenkyns, H.C. (1974) Origin of red nodular limestones (Ammonitico Rosso, Knollenkalke) in the Mediterranean Jurassic: a diagenetic model. In: *Pelagic Sediments: on Land and Under the Sea* (Eds. Hsü, K.J. and Jenkyns, H.C.), pp. 249–271. Blackwell Scientific Publications, Oxford.

Jerolmack, D.J. and **Sadler, P.** (2007) Transience and persistence in the depositional record of continental margins. *J. Geophys. Res. Ser. F*, **112**, F03S13.

Juračić, M., **Benac, Č.** and **Crmarić, R.** (1999) Seabed and surface sediment map of the Kvarner Region, Adriatic Sea, Croatia (Lithological map, 1: 500,000). *Geol. Croatica*, **52**, 131–140.

Kaczmarek, S.E., **Fullmer, S.M.** and **Hasiuk, F.J.** (2015) A universal classification scheme for the microcrystals that host limestone microporosity. *J. Sed. Res.*, **85**, 1197–1212.

Kemp, D.B. (2012) Stochastic and deterministic controls on stratigraphic completeness and fidelity. *Int. J. Earth Sci.*, **101**, 2225–2238.

Kemp, D.B., **Fraser, W.T.** and **Izumi, K.** (2018) Stratigraphic completeness and resolution in an ancient mudrock succession. *Sedimentology*, **65**, 1875–1890.

Kennedy, W.J. and **Garrison, R.E.** (1975) Morphology and genesis of nodular chalks and hardgrounds in the Upper Cretaceous of southern England. *Sedimentology*, **22**, 311–386.

Kidwell, S.M. (1986) Models for fossil concentrations: paleobiologic implications. *Paleobiology*, **12**, 6–24.

Kidwell, S.M. (1989) Stratigraphic condensation of marine transgressive records: origin of major shell deposits in the Miocene of Maryland. *J. Geol.*, **97**, 1–24.

Kidwell, S.M. (1991a) The stratigraphy of shell concentrations. In: *Taphonomy: Releasing the Data Locked in the Fossil Record* (Eds Allison, P.A. and Briggs, D.E.G.), *Topics in Geobiology* **9**, 211–290.

Kidwell, S.M. (1991b) Taphonomic feedback (live/dead interactions) in the genesis of bioclastic beds: keys to reconstructing sedimentary dynamics. In: *Cycles and Events in Stratigraphy* (Eds Einsele, G., Ricken, W. and Seilacher, A.), pp. 268–282. Springer-Verlag, Heidelberg.

Kidwell, S.M. (1993) Taphonomic expressions of sedimentary hiatuses: field observations on bioclastic concentrations and sequence anatomy in low, moderate and high subsidence settings. *Geol. Rundsch.*, **82**, 189–202.

Kidwell, S.M. (1997) Time-averaging in the marine fossil record: overview of strategies and uncertainties. *Geobios*, **30**, 977–995.

Kidwell, S.M., **Best, M.M.** and **Kaufman, D.S.** (2005) Taphonomic trade-offs in tropical marine death assemblages: differential time averaging, shell loss, and probable bias in siliciclastic vs. carbonate facies. *Geology*, **33**, 729–732.

Kondo, Y., **Abbott, S.T.**, **Kitamura, A.**, **Kamp, P.J.**, **Naish, T.R.**, **Kamataki, T.** and **Saul, G.S.** (1998) The relationship between shellbed type and sequence architecture: examples from Japan and New Zealand. *Sed. Geol.*, **122**, 109–127.

Kowalewski, M. and **Bambach, R.K.** (2003) The limits of paleontological resolution. In: *Approaches in High-Resolution Stratigraphic Paleontology* (Ed. Harries, P.J.), *Topics in Geobiology*, **21**, 1–48.

Ku, T.C.W., **Walter, L.M.**, **Coleman, M.L.**, **Blake, R.E.** and **Martini, A.M.** (1999) Coupling between sulfur recycling and syndepositional carbonate dissolution: evidence from oxygen and sulfur isotope composition of pore water sulfate, South Florida Platform, USA. *Geochim. Cosmochim. Acta*, **63**, 2529–2546.

Macintyre, I.G. and **Aronson, R.B.** (2006) Lithified and unlithified Mg-calcite precipitates in tropical reef environments. *J. Sed. Res.*, **76**, 81–90.

Madof, A.S., **Harris, A.D.** and **Connell, S.D.** (2016) Nearshore along-strike variability: is the concept of the systems tract unhinged? *Geology*, **44**, 315–318.

Massari, F. and **D'Alessandro, A.** (2012) Facies partitioning and sequence stratigraphy of a mixed siliciclastic-carbonate ramp stack in the Gelasian of Sicily (S Italy): A potential model for icehouse, distally-steepened heterozoan ramps. *Riv. Ital. Paleontol. Stratigr.*, **118**, 503–534.

McKinney, F.K. and **Jaklin, A.** (2001) Sediment accumulation in a shallow-water meadow carpeted by a small erect bryozoan. *Sed. Geol.*, **145**, 397–410.

McLaughlin, P.I., **Brett, C.E.** and **Wilson, M.A.** (2008) Hierarchy of sedimentary discontinuity surfaces and condensed beds from the middle Paleozoic of eastern North America: implications for cratonic sequence stratigraphy. *Geol. Assoc. Can. Spec. Pap.*, **48**, 175–200.

Meister, P., **Wiedling, J.**, **Lott, C.**, **Bach, W.**, **Kuhfuß, H.**, **Wegener, G.**, **Böttcher, M.E.**, **Deusner, C.**, **Lichtschlag, A.**, **Bernasconi, S.M.** and **Weber, M.** (2018) Anaerobic methane oxidation inducing carbonate precipitation at abiogenic methane seeps in the Tuscan archipelago (Italy). *PLoS One*, **13**, e0207305.

Meldahl, K.H., **Flessa, K.W.** and **Cutler, A.H.** (1997) Time-averaging and postmortem skeletal survival in benthic fossil assemblages: quantitative comparisons among Holocene environments. *Paleobiology*, **23**, 207–229.

Meyers, S.R. and **Sageman, B.B.** (2004) Detection, quantification, and significance of hiatuses in pelagic and hemipelagic strata. *Earth Planet. Sci. Lett.*, **224**, 55–72.

Michel, J., **Laugié, M.**, **Pohl, A.**, **Lanteaume, C.**, **Masse, J.P.**, **Donnadieu, Y.** and **Borgomano, J.** (2019) Marine carbonate factories: a global model of carbonate platform distribution. *Int. J. Earth Sci.*, **108**, 1773–1792.

Milliman, J.D. and **Müller, J.** (1973) Precipitation and lithification of magnesian calcite in the deep-sea sediments of the eastern Mediterranean Sea. *Sedimentology*, **20**, 29–45.

Moore, T.C., **Van Andel, T.H.**, **Sancetta, C.** and **Pisias, N.G.** (1978) Cenozoic hiatuses in pelagic sediments. *Micropaleontology*, **24**, 113–138.

Morad, S., **Ketzer, J.M.** and **De Ros, L.F.** (2012) Linking diagenesis to sequence stratigraphy: an integrated tool for understanding and predicting reservoir quality distribution. In: *Linking Diagenesis to Sequence Stratigraphy* (Eds Morad, S., Ketzer, J.M. and de Ros, L.F.), *Special Publication of the International Association of Sedimentologists*, **45**, 1–36.

Morton, B. (2009) Aspects of the biology and functional morphology of *Timoclea ovata* (Bivalvia: Veneroidea: Venerinae) in the Azores, Portugal, and a comparison with Chione elevata (Chioninae). *Açoreana*, **6**, 105–119.

Moscon, G., **Correggiari, A.**, **Stefani, C.**, **Fontana, A.** and **Remia, A.** (2015) Very-high resolution analysis of a transgressive deposit in the Northern Adriatic Sea (Italy). *Alpine Mediterr. Quatern.*, **28**, 121–129.

Munnecke, A. and **Samtleben, C.** (1996) The formation of micritic limestones and the development of limestone-marl alternations in the Silurian of Gotland, Sweden. *Facies*, **34**, 159–176.

Mutti, M. and **Bernoulli, D.** (2003) Early marine lithification and hardground development on a Miocene ramp (Maiella, Italy): key surfaces to track changes in trophic resources in nontropical carbonate settings. *J. Sed. Res.*, **73**, 296–308.

Naish, T. and **Kamp, P.J.** (1997) Sequence stratigraphy of sixth-order (41 ky) Pliocene-Pleistocene cyclothems, Wanganui basin, New Zealand: a case for the regressive systems tract. *Geol. Soc. Am. Bull.*, **109**, 978–999.

Nelson, C.S. and **James, N.P.** (2000) Marine cements in mid-Tertiary cool-water shelf limestones of New Zealand and southern Australia. *Sedimentology*, **47**, 609–629.

Nohl, T. and **Munnecke, A.** (2019) Reconstructing time and diagenesis of limestone-marl alternations from the selective compaction of colonies of the tabulate coral Halysites. *Bull. Geosci.*, **94**, 279–298.

Novak, A., **Šmuc, A.**, **Poglajen, S.**, **Celarc, B.** and **Vrabec, M.** (2020a) Sound velocity in a thin shallowly submerged terrestrial-marine Quaternary succession (northern Adriatic Sea). *Water*, **12**, 560.

Novak, A., **Šmuc, A.**, **Poglajen, S.** and **Vrabec, M.** (2020b) Linking the high-resolution acoustic and sedimentary facies of a transgressed Late Quaternary alluvial plain (Gulf of Trieste, northern Adriatic). *Mar. Geol.*, **419**, 106061.

Ogrinc, N. and **Faganeli, J.** (2003) Stable carbon isotopes in pore waters of coastal marine sediments (the Gulf of Trieste, N Adriatic). *Acta Chim. Slov.*, **50**, 645–662.

O'Leary, M.J., **Perry, C.T.**, **Beavington-Penney, S.J.** and **Turner, J.R.** (2009) The significant role of sediment bio-retexturing within a contemporary carbonate platform system: Implications for carbonate microfacies development. *Sed. Geol.*, **219**, 169–179.

Olszewski, T.D. (2004) Modeling the influence of taphonomic destruction, reworking, and burial on time-averaging in fossil accumulations. *Palaios*, **19**, 39–50.

Palmer, T. and **Wilson, M.** (2004) Calcite precipitation and dissolution of biogenic aragonite in shallow Ordovician calcite seas. *Lethaia*, **37**, 417–427.

Paul, A. and **Lokier, S.W.** (2017) Holocene marine hardground formation in the Arabian Gulf: shoreline stabilisation, sea level and early diagenesis in the coastal sabkha of Abu Dhabi. *Sed. Geol.*, **352**, 1–13.

Pedley, M. and **Grasso, M.** (2002) Lithofacies modelling and sequence stratigraphy in microtidal cool-water carbonates: a case study from the Pleistocene of Sicily, Italy. *Sedimentology*, **49**, 533–553.

Pellegrini, C., **Maselli, V.**, **Cattaneo, A.**, **Piva, A.**, **Ceregato, A.** and **Trincardi, F.** (2015) Anatomy of a compound delta from the post-glacial transgressive record in the Adriatic Sea. *Mar. Geol.*, **362**, 43–59.

Pemberton, S.G., **MacEachern, J.A.** and **Saunders, T.** (2004) Stratigraphic applications of substrate-specific ichnofacies: delineating discontinuities in the rock record. *Geol. Soc. London Spec. Publ.*, **228**, 29–62.

Perry, C.T. (1999) Biofilm-related calcification, sediment trapping and constructive micrite envelopes: a criterion for the recognition of ancient grass-bed environments? *Sedimentology*, **46**, 33–45.

Pervesler, P. and **Hohenegger, J.** (2006) Orientation of crustacean burrows in the Bay of Panzano (Gulf of Trieste, northern Adriatic Sea). *Lethaia*, **39**, 173–186.

Peters, S.E. (2006) Genus extinction, origination, and the durations of sedimentary hiatuses. *Paleobiology*, **32**, 387–407.

Petro, S.M., **Ritter, M.D.N.**, **Pivel, M.A.G.** and **Coimbra, J.C.** (2018) Surviving in the water column: Defining the taphonomically active zone in pelagic systems. *Palaios*, **33**, 85–93.

Plet, C., **Grice, K.**, **Pagès, A.**, **Ruebsam, W.**, **Coolen, M.J.L.** and **Schwark, L.** (2016) Microbially-mediated fossil-bearing carbonate concretions and their significance for palaeoenvironmental reconstructions: a multi-proxy organic and inorganic geochemical appraisal. *Chem. Geol.*, **426**, 95–108.

Pomar, L. and **Haq, B.U.** (2016) Decoding depositional sequences in carbonate systems: concepts vs experience. *Glob. Planet. Change*, **146**, 190–225.

Powell, E.N., **Brett, C.E.**, **Parsons-Hubbard, K.M.**, **Callender, W.R.**, **Staff, G.M.**, **Walker, S.E.**, **Raymond, A.** and **Ashton-Alcox, K.A.** (2011) The relationship of bionts and taphonomic processes in molluscan taphofacies formation on the continental shelf and slope: eight-year trends: Gulf of Mexico and Bahamas. *Facies*, **57**, 15–37.

Powell, E.N. and **Davies, D.J.** (1990) When is an "old" shell really old? *J. Geol.*, **98**, 823–844.

Pufahl, P.K. and **Grimm, K.A.** (2003) Coated phosphate grains: proxy for physical, chemical, and ecological changes in seawater. *Geology*, **31**, 801–804.

R Core Team. (2018) *R: A Language and Environment for Statistical Computing*. R Foundation for Statistical Computing, Vienna, Austria. https://www.R-project.org/

Raiswell, R. (1988) Chemical model for the origin of minor limestone-shale cycles by anaerobic methane oxidation. *Geology*, **16**, 641–644.

Raiswell, R. and **Fisher, Q.J.** (2004) Rates of carbonate cementation associated with sulphate reduction in DSDP/ODP sediments: implications for the formation of concretions. *Chem. Geol.*, **211**, 71–85.

Reid, R.P., **Macintyre, I.G.** and **James, N.P.** (1990) Internal precipitation of microcrystalline carbonate: a fundamental problem for sedimentologists. *Sed. Geol.*, **68**, 163–170.

Reid, R.P. and **Macintyre, I.G.** (1998) Carbonate recrystallization in shallow marine environments: a widespread diagenetic process forming micritized grains. *J. Sed. Res.*, **68**, 928–946.

Ritter, M.D.N., **Erthal, F.**, **Kosnik, M.**, **Coimbra, J.C.** and **Kaufman, D.S.** (2017) Spatial variation in the temporal resolution of subtropical shallow-water molluscan death assemblages. *Palaios*, **32**, 572–583.

Sadler, P.M. (1981) Sediment accumulation rates and the completeness of stratigraphic sections. *Journal of Geology*, **89**, 569–584.

Sanders, D. (2001) Burrow-mediated carbonate dissolution in rudist biostromes (Aurisina, Italy): implications for taphonomy in tropical, shallow subtidal carbonate environments. *Palaeogeogr. Palaeoclimatol. Palaeoecol.*, **168**, 39–74.

Scarponi, D., **Azzarone, M.**, **Kusnerik, K.**, **Amorosi, A.**, **Bohacs, K.M.**, **Drexler, T.M.** and **Kowalewski, M.** (2017) Systematic vertical and lateral changes in quality and time resolution of the macrofossil record: insights from Holocene transgressive deposits, Po coastal plain, Italy. *Mar. Pet. Geol.*, **87**, 128–136.

Scarponi, D., **Kaufman, D.**, **Amorosi, A.** and **Kowalewski, M.** (2013) Sequence stratigraphy and the resolution of the fossil record. *Geology*, **41**, 239–242.

Schiffbauer, J.D., **Xiao, S.**, **Cai, Y.**, **Wallace, A.F.**, **Hua, H.**, **Hunter, J.**, **Xu, H.**, **Peng, Y.** and **Kaufman, A.J.** (2014) A unifying model for Neoproterozoic-Palaeozoic exceptional fossil preservation through pyritization and carbonaceous compression. *Nat. Commun.*, **5**, 1–12.

Schlager, W. (1991) Depositional bias and environmental change—important factors in sequence stratigraphy. *Sed. Geol.*, **70**, 109–130.

Schlager, W., **Reijmer, J.J.** and **Droxler, A.** (1994) Highstand shedding of carbonate platforms. *J. Sed. Res.*, **64**, 270–281.

Schnedl, S.M., **Haselmair, A.**, **Gallmetzer, I.**, **Mautner, A.K.**, **Tomašových, A.** and **Zuschin, M.** (2018) Molluscan benthic communities at Brijuni Islands (northern Adriatic Sea) shaped by Holocene sea-level rise and recent human eutrophication and pollution. *Holocene*, **28**, 1801–1817.

Seneš, J. (1989) North Adriatic inter-island shelf ecosystems of the Rovinj area. *Geol. Carpath.*, **40**, 333–354.

Storms, J.E., **Weltje, G.J.**, **Terra, G.J.**, **Cattaneo, A.** and **Trincardi, F.** (2008) Coastal dynamics under conditions of rapid sea-level rise: Late Pleistocene to Early Holocene evolution of barrier–lagoon systems on the northern Adriatic shelf (Italy). *Quatern. Sci. Rev.*, **27**, 1107–1123.

Strasser, A. (2015) Hiatuses and condensation: an estimation of time lost on a shallow carbonate platform. *Depos. Rec.*, **1**, 91–117.

Straub, K.M., **Duller, R.A.**, **Foreman, B.Z.** and **Hajek, E.A.** (2020) Buffered, incomplete, and shredded: the challenges of reading an imperfect stratigraphic record. *J. Geophys. Res., Ser. F*, **125**, e2019JF005079.

Taviani, M., **Franchi, F.**, **Angeletti, L.**, **Correggiari, A.**, **López-Correa, M.**, **Maselli, V.**, **Mazzoli, C.** and **Peckmann, J.** (2015) Biodetrital carbonates on the Adriatic continental shelf imprinted by oxidation of seeping hydrocarbons. *Mar. Petrol. Geol.*, **66**, 511–531.

Taylor, K.G. and **Machent, P.G.** (2010) Systematic sequence-scale controls on carbonate cementation in a siliciclastic sedimentary basin: examples from Upper Cretaceous shallow marine deposits of Utah and Coloradao, USA. *Mar. Petrol. Geol.*, **27**, 1297–1310.

Tipper, J.C. (2016) Measured rates of sedimentation: what exactly are we estimating, and why? *Sed. Geol.*, **339**, 151–171.

Tomašových, A., **Fürsich, F.T.** and **Olszewski, T.D.** (2006) Modeling shelliness and alteration in shell beds: variation in hardpart input and burial rates leads to opposing predictions. *Paleobiology*, **32**, 278–298.

Tomašových, A., **Gallmetzer, I.**, **Haselmair, A.**, **Kaufman, D.S.**, **Mavrič, B.** and **Zuschin, M.** (2019b) A decline in molluscan carbonate production driven by the loss of vegetated habitats encoded in the Holocene sedimentary record of the Gulf of Trieste. *Sedimentology*, **66**, 781–807.

Tomašových, A., **Kidwell, S.M.**, **Barber, R.F.** and **Kaufman, D.S.** (2014) Long-term accumulation of carbonate shells reflects a 100-fold drop in loss rate. *Geology*, **42**, 819–822.

Tomašových, A., **Kidwell, S.M.**, **Alexander, C.R.** and **Kaufman, D.S.** (2019a) Millennial-scale age offsets within fossil assemblages: result of bioturbation below the taphonomic active zone and out-of-phase production. *Paleoceanogr. Paleoclimatol.*, **34**, 954–977.

Tomašových, A. and **Schlögl, J.** (2008) Analyzing variations in cephalopod abundances in shell concentrations: the combined effects of production and density-dependent cementation rates. *Palaios*, **23**, 648–666.

Tomašových, A., **Schlögl, J.**, **Kaufman, D.S.** and **Hudáčková, N.** (2016) Temporal and bathymetric resolution of nautiloid death assemblages in stratigraphically condensed oozes (New Caledonia). *Terra Nova*, **28**, 271–278.

Tomašových, A., **Schlögl, J.**, **Biroň, A.**, **Hudáčková, N.** and **Mikuš, T.** (2017) Taphonomic clock and bathymetric dependence of cephalopod preservation in bathyal, sediment-starved environments. *Palaios*, **32**, 135–152.

Toscano, F. and **Sorgente, B.** (2002) Rhodalgal-bryomol temperate carbonates from the Apulian Shelf (Southeastern Italy), relict and modern deposits on a current dominated shelf. *Facies*, **46**, 103–118.

Trampush, S.M. and **Hajek, E.A.** (2017) Preserving proxy records in dynamic landscapes: modeling and examples from the Paleocene-Eocene Thermal Maximum. *Geology*, **45**, 967–970.

Trincardi, F., **Correggiari, A.** and **Roveri, M.** (1994) Late Quaternary transgressive erosion and deposition in a modern epicontinental shelf: the Adriatic semienclosed basin. *Geo-Mar. Lett.*, **14**, 41–51.

Van der Kooij, B., **Immenhauser, A.**, **Steuber, T.**, **Bahamonde Rionda, J.R.** and **Merino Tome, O.** (2010) Controlling factors of volumetrically important marine carbonate cementation in deep slope settings. *Sedimentology*, **57**, 1491–1525.

Vodrážka, R., **Sklenář, J.**, **Čech, S.**, **Laurin, J.** and **Hradecká, L.** (2009) Phosphatic intraclasts in shallow-water hemipelagic strata: a source of palaeoecological, taphonomic and biostratigraphic data (Upper Turonian, Bohemian Cretaceous Basin). *Cretaceous Research*, **30**, 204–222.

Walter, L.M., **Bischof, S.A.**, **Patterson, W.P.** and **Lyons, T.W.** (1993) Dissolution and recrystallization in modern shelf carbonates: evidence from pore water and solid phase chemistry. *Philos. Trans. R. Soc. London*, **A344**, 27–36.

Weedon, G.P., **Jenkyns, H.C.** and **Page, K.N.** (2018) Combined sea-level and climate controls on limestone formation, hiatuses and ammonite preservation in the Blue Lias Formation, South Britain (uppermost Triassic-Lower Jurassic). *Geol. Mag.*, **155**, 1117–1149.

Wetzel, A. and **Allia, V.** (2000) The significance of hiatus beds in shallow-water mudstones: an example from the Middle Jurassic of Switzerland. *J. Sed. Res.*, **70**, 170–180.

Wheeley, J.R., **Cherns, L.** and **Wright, V.P.** (2008) Provenance of microcrystalline carbonate cement in limestone–marl alternations (LMA): aragonite mud or molluscs? *J. Geol. Soc.*, **165**, 395–403.

Wilson, M.A., **Zatoń, M.** and **Avni, Y.** (2012) Origin, palaeoecology and stratigraphic significance of bored and encrusted concretions from the Upper Cretaceous (Santonian) of southern Israel. *Palaeobiodivers. Palaeoenviron.*, **92**, 343–352.

Yanes, Y., **Kowalewski, M.**, **Ortiz, J.E.**, **Castillo, C.**, **de Torres, T.** and **de la Nuez, J.** (2007) Scale and structure of time-averaging (age mixing) in terrestrial gastropod assemblages from Quaternary eolian deposits of the eastern Canary Islands. *Palaeogeogr. Palaeoclimatol. Palaeoecol.*, **251**, 283–299.

Zamora, S., **Mayoral, E.**, **Vintaned, J.A.G.**, **Bajo, S.** and **Espílez, E.** (2008) The infaunal echinoid Micraster: taphonomic pathways indicated by sclerozoan trace and body fossils from the Upper Cretaceous of northern Spain. *Geobios*, **41**, 15–29.

Zecchin, M. and **Catuneanu, O.** (2013) High-resolution sequence stratigraphy of clastic shelves I: units and bounding surfaces. *Mar. Petrol. Geol.*, **39**, 1–25.

Zecchin, M. and **Catuneanu, O.** (2017) High-resolution sequence stratigraphy of clastic shelves VI: mixed siliciclastic-carbonate systems. *Mar. Petrol. Geol.*, **88**, 712–723.

Zecchin, M., **Gordini, E.** and **Ramella, R.** (2015) Recognition of a drowned delta in the northern Adriatic Sea, Italy: stratigraphic characteristics and its significance in the frame of the early Holocene sea-level rise. *Holocene*, **25**, 1027–1038.

Zecchin, M., **Mellere, D.** and **Roda, C.** (2006) Sequence stratigraphy and architectural variability in growth fault-bounded basin fills: a review of Plio-Pleistocene stratal units of the Crotone Basin, southern Italy. *J. Geol. Soc. London*, **163**, 471–486.

Zhang, S. (2020) The relationship between organoclastic sulfate reduction and carbonate precipitation/dissolution in marine sediments. *Mar. Geol.*, **428**, 106284.

Zhu, Q., **Aller, R.C.** and **Fan, Y.** (2006) Two-dimensional pH distributions and dynamics in bioturbated marine sediments. *Geochim. Cosmochim. Acta*, **70**, 4933–4949.

Zuschin, M. and **Stachowitsch, M.** (2009) Epifauna-dominated benthic shelf assemblages: lessons from the modern Adriatic Sea. *Palaios*, **24**, 211–221.

Manuscript received 5 December 2020; revision accepted 26 July 2021

Supporting Information

Additional information may be found in the online version of this article:

Figure S1. Individual-level ordinations (principal coordinate analyses, based on Manhattan distances and eight alteration variables) of dated *Timoclea ovata* valves in four stratigraphic units (at M44 and M40) shows high variation in alteration within the surface mixed layer (A) and within the three subsurface unit (B) and (D).

Table S1. Amino acid racemization (AAR) data of dated valves of *T. ovata* from M44 and M40 and their taphonomic scores.

Table S2. The conventional and calibrated ^{14}C ages of bivalves from M40 (new data) and M44 (published in Schnedl *et al.,* 2018).

Table S3. Final age model with mean per-increment age of dated increments, long-term sedimentation rate, and expected and observed time averaging (inter-quartile age range).

Table S4. Cohort-level taphonomic clock based on Pearson correlations and generalized linear models in which the frequency of valves in 100-year cohorts (in valves <1000 years old) and in 500-year cohorts (in valves >1000 years old) is regressed or correlated with postmortem age in the fully-mixed layer and in the highstand unit.

Table S5. Assemblage-level taphonomic clock between the relative frequencies of seven alteration variables (and the mean of the per-valve sum of seven alteration variables) in 5 cm increments and their time averaging measured with Spearman rank correlation.

Appendix S1. R language script for analyses of assemblage-level alteration and taphonomic clock at individual, cohort, and assemblage scales.

Appendix S2. R language script for modeling the effects of variable sedimentation rates on time averaging with the random walk model.